DESIGN OF A FOLDING TAIL FIN FOR A TACTICAL MISSILE

TAKTİK BİR FÜZE İÇİN KATLANIR KUYRUK TASARIMI

ALİ ANIL DİNLER

PROF. DR BORA YILDIRIM

Supervisor

Submitted to
Graduate School of Science and Engineering of Hacettepe University
as a Partial Fulfillment to the Requirements
for the Award of the Degree of Master of Science
in Mechanical Engineering.

2024

To my family and loved ones...

ABSTRACT

DESIGN OF A FOLDING TAIL FIN FOR A TACTICAL MISSILE

Ali Anıl DİNLER

Master of Science Degree, Department of Mechanical Engineering
Supervisor: Prof. Dr. Bora YILDIRIM
May 2024, 73 pages

Guided missiles are generally stored in missile canisters during storage, handling and transit up to missiles are fired. In system design perspective, the design requirements of missiles are defined beforehand and assigned. Due to space, weight, transportation, launch cell limitations, it is not possible to increase dimensions of missile canisters. Because of this reason, missile packaging is directly affected by canister dimensions. Since the missile extremities are defined by wing, canard, tail or control surfaces; It is necessary to fold those parts to fit into canisters while decreasing the space occupied. In this study design of a folding tail fin mechanism has been carried out. Details of design, analysis, manufacturing and test procedures will be examined.

Keywords: Folding Tail Fin Mechanism, Missile, Canister, Aerodynamic Analysis, Structural Analysis, Dynamic Analysis, Manufacturing, Validation Tests

ÖZET

TAKTİK BİR FÜZE İÇİN KATLANIR KUYRUK TASARIMI

Ali Anıl DİNLER

Yüksek Lisans, Makine Mühendisliği Bölümü
Tez Danışmanı: Prof. Dr. Bora YILDIRIM
Mayıs 2024, 73 sayfa

Füzeler ateşlenene kadar depolama, idame ve taşıma durumlarında genellikle kanister içerisinde muhafaza edilmektedir. Sistem dizayn bakış açısıyla bakıldığında füzenin tasarım gereklilikleri öncesinden belirlenip atanmaktadır. Mesafe, ağırlık, taşıma ve atış hücresinin limitleri gibi nedenlerle kanisterin boyutlarını artırmak mümkün değildir. Bu nedenden dolayı füze paketlemesi doğrudan kanister ölçülerinden etkilenmektedir. Füzenin sınır noktaları kanat, kanard, kuyruk yada kontrol yüzeyleri tarafından tanımlandığından dolayı, bu parçaları katlayıp daha az yer işgal ederek kanister içerisine sığmak gerekmektedir. Bu çalışmada katlanır kuyruk tasarımı gerçekleştirilmiştir. Tasarım, analiz, imalat ve test prosedürlerinin detayları paylaşılacaktır.

Anahtar Kelimeler: Katlanır Kuyruk Mekanizması, Füze, Kanister, Aerodinamik Analiz, Yapısal Analiz, Dinamik Analiz, İmalat, Validasyon Testleri

ACKNOWLEDGMENTS

Foremost, I would like to express my deepest appreciation to all those who provided me with the possibility to complete this thesis.

This work would not have been possible without the guidance of my supervisor Prof. Dr. Bora YILDIRIM. I am grateful for his endless support.

I also would like to thank to my family; my parents and my elder sister for their continued love, patience and encouragement throughout the thesis period.

TABLE OF CONTENT

ABSTRACT i

ACKNOWLEDGMENTS iii

TABLE OF CONTENT iv

LIST OF FIGURES vi

LIST OF TABLES ix

NOMENCLATURE x

1. INTRODUCTION 1

2. LITERATURE REVIEW 3

2.1. Classification of Missiles 3

2.1.1. Based on Guidance 3

2.1.2. Based on Method of Launching 4

2.1.3. Based on Range 5

2.1.4. Based on Aerodynamic Control 6

2.2. Classification of Folding Mechanisms 7

2.2.1. Bendable/Flexible Members 7

2.2.2. Motor Driven Mechanisms 9

2.2.3. Spring Powered Mechanisms 9

2.2.4. Pneumatic/Hydraulic Powered Mechanisms 13

2.2.5. Double Swing Self Erecting Mechanisms 14

2.2.6. Pyrotechnic Driven Mechanism 17

2.2.7. Torsion Bar Mechanisms 17

2.2.8. Leaf Spring Mechanisms 18

2.2.9. Miscellaneous Systems 20

3. MATERIAL AND METHOD 21

4. RESULTS AND DISCUSSION 23

4.1. Analytical Calculations 23

4.1.1. Calculation of Torsion Spring 23
4.1.2. Calculation of Deployment Time 27
4.2. Performed Analyses 29
4.2.1. Computational Fluid Dynamics Analysis 29
4.2.2. Structural Analysis 41
4.2.3. Dynamic Analysis 46
4.2.4. Fatigue Analysis 49
4.3. Performed Tests 54
4.3.1. Aerodynamic Loading Test 54
4.3.2. Structural Integrity Test 57
4.3.3. Deployment Time Test 58
5. CONCLUSION 62
6. REFERENCES 64
APPENDICES 66
Appendix A – Approximation of Total Deployment Time 66
Appendix B – Originality Report 72
CURRICULUM VİTAE 73

LIST OF FIGURES

Figure 1 Missile Classification by Method of Launching[2] 5
Figure 2 Types of Control Configurations[3] 6
Figure 3 Isometric View of the Missile 7
Figure 4 Bendable/Flexible Wings[4] 8
Figure 5 Integration of Bendable System[4] 8
Figure 6 Extendable Wing Mechanism[5] 9
Figure 7 Torsion Spring Mechanism[6] 10
Figure 8 Latching Mechanism of a Folding Missile Wings[7] 11
Figure 9 Arcuate Plunger Driven by Compression Spring[8] 11
Figure 10 Dual Sliding Fin Lock Mechanism[9] 12
Figure 11 Tension Spring Mechanism[10] 12
Figure 12 Cam Follower Mechanism[11] 13
Figure 13 Gas Pressure Spring[12] 14
Figure 14 Turntable Folding Fin Mechanism[13] 14
Figure 15 Missile Appendage Deployment Mechanism[14] 15
Figure 16 Self Erecting Wing[15] 15
Figure 17 Conformal Wing Geometry[15] 16
Figure 18 Solenoid Retainer Mechanism[15] 16
Figure 19 Trunnion Lock[15] 16
Figure 20 Pyrotechnic Driven Mechanism[16] 17
Figure 21 Torsion Bar Mechanism[17] 17
Figure 22 Double Torsion Bar Longitudinal Mechanism[18] 18
Figure 23 Leaf Spring Folding Mechanism[19] 19
Figure 24 Leaf Spring Design with Different Fixation Element[20] 19
Figure 25 A Passive Deployment Apparatus[21] 20
Figure 26 A Scotch Yoke Deployment Device[22] 20
Figure 27 Folded Tail Fins View in Canister 21
Figure 28 Design of Folding Tail Fin Deployment Test Fixture 22
Figure 29 Cross Section of Square Shaped Torsion Spring 23
Figure 30 Spring Rate Test Fixture 24
Figure 31 Torque Reading 25
Figure 32 Spring #1 Test Result 26
Figure 33 Spring #2 Test Result 26
Figure 34 Rotating Body of the Folding Tail Fin 27
Figure 35 Predesign of Folding Tail Fin 28

Figure 36 Isometric View of Torsion Spring 28
Figure 37 Typical Wing Planforms[2] 29
Figure 38 Modified Double Wedge Airfoil Section 30
Figure 39 Named Selection of Analysis Model 30
Figure 40 Flow Domain Around the Body 31
Figure 41 Dimensions of Fluid Domain 31
Figure 42 SC Model Transfer to Ansys Fluent Meshing 32
Figure 43 Surface Meshes and Local Sizing 32
Figure 44 Fluid Region Geometry Type 33
Figure 45 Boundary Types 33
Figure 46 Volumetric Mesh 35
Figure 47 Boundary Layers Around the Walls 35
Figure 48 Properties of Fluid 36
Figure 49 Viscosity Model 37
Figure 50 X and Y Components of Flow Direction 38
Figure 51 K-Omega SST Model Setup 38
Figure 52 Pressure Distribution of Upper Surface 39
Figure 53 Pressure Distribution of Lower Surface 39
Figure 54 Velocity Distribution of the Bottom Surface 40
Figure 55 Lift Force and Bending Moment Values 40
Figure 56 FSI Analysis Model 41
Figure 57 Fixed Support Boundary Condition 42
Figure 58 Imported Pressure Initial Time Step 42
Figure 59 Imported Aerodynamic Pressures 42
Figure 60 Static Structural Preprocess Setup 43
Figure 61 Element Quality 43
Figure 62 Total Deformation of Folding Tail Fin 44
Figure 63 Equivalent Stress Distribution on the Airfoil Body 44
Figure 64 Reaction Force of the Airfoil 45
Figure 65 3D Model on MSC Adams 46
Figure 66 Simplified Dynamic Model 46
Figure 67 Torsion Springs and Compression Springs 47
Figure 68 Flexible Connection Assignments 47
Figure 69 Material Assignment 48
Figure 70 Deployment Time 48
Figure 71 Fatigue Properties of 17-4 PH H-1050 Stainless Steel 49
Figure 72 S-N Curve of 17-4 PH H-1050 Stainless Steel 50
Figure 73 Discretization of the Torsion Spring 50
Figure 74 Boundary Conditions of Torsion Spring 51

Figure 75 Fatigue Analysis Settings 51
Figure 76 Mean Stress Correction Theory 52
Figure 77 Equivalent Stress Distribution on Torsion Spring 52
Figure 78 Directional Deformation on Torsion Spring 53
Figure 79 Safety Factor of Torsion Spring 53
Figure 80 Lower and Upper Cp Points 55
Figure 81 Aerodynamical Loading Test Setup 56
Figure 82 Structural Integrity Test 57
Figure 83 Deployment Time Test Fixture 58
Figure 84 Fin Position for Different Angles 59
Figure 85 Angle vs Time Graph of Deployment Test 61

LIST OF TABLES

Table 1 Spring Constant Test Matrix 25
Table 2 Input Parameters for Deployment Time 28
Table 3 Dimensions of the Model 31
Table 4 Wall Distance Estimation Parameters 34
Table 5 Turbulence Flow Parameters 34
Table 6 Mesh Statistics 36
Table 7 Static Condition Parameters 38
Table 8 Force and Moment Reaction at Fixed Support 45
Table 9 Spring Constants 47
Table 10 Joint Assignment of the Airfoil Bodies 48
Table 11 Exported Aerodynamical Pressure Data of Each Element 54
Table 12 Cp & Fn Values of Upper and Lower Airfoil Body 55
Table 13 Summary Table of Aerodynamical Loading Test 56
Table 14 Structural Integrity Test Results 58
Table 15 High Speed Camera Deployment Time Test Summary 59
Table 16 High Speed Camera Deployment Test Results 59
Table 17 Analyses and Tests Results Comparison Table 63

NOMENCLATURE

Symbols

Cg	Center of Gravity
C_f	Skin Friction Coefficient
Cp	Center of Pressure
d	Thickness (m)
D	Coil Average Diameter (m)
E	Young Modulus (GPa)
I	Moment of Inertia (kgm^2)
k	Spring Constant (Nm/rad)
k_{eq}	Equivalent Spring Constant (Nm/rad)
M	Mach
N	Number of Active Coils
p	Pressure (Pa)
p_0	Total Pressure (Pa)
Re	Reynolds Number
S	Sutherland Constant (K)
T	Torque (Nm)
T_0	Total Temperature (K)
U_τ	Friction Velocity (m/s)
U_∞	Freestream Velocity (Mach)
y	Wall Distance (m)
y^+	Dimensionless Wall Distance
θ	Angular Displacement (rad)
μ	Dynamic Viscosity (kg/ms)

μ_0	Reference Viscosity (kg/ms)
ρ	Density (kg/m^3)
σ	Bending Stress [MPa]
τ_w	Wall Shear Stress (kg/(ms^2))
Φ	Angle of Twist [deg]
ω	Angular Velocity(rad/s)

Abbreviations

AAM	Air to Air Missile
AoA	Angle of Atack
ASM	Air to Surface Missile
CAD	Computer Aided Design
CFD	Computational Fluid Dynamics
DOF	Degrees of Freedom
EDM	Electro Discharge Machining
ERSAM	Extended Range Surface to Air Missile
FAI	First Article Inspection
FSI	Fluid to Solid Interface
ICBM	Intercontinental Ballistic Missile
LRSAM	Long Range Surface to Air Missile
MRSAM	Medium Range Surface to Air Missile
SAM	Surface to Air Missile
SC	SpaceClaim
SRM	Solid Rocket Motor
SRSAM	Short Range Surface to Air Missile

SSM	Surface to Surface Missile
UAV	Unmanned Aerial Vehicle
3D	Three Dimensional

1. INTRODUCTION

Missiles are key elements to strike an enemy unit from distance. As such they are considered as an extension of artillery in the early stages. The earliest recorded use of rockets in warfare was at the military siege of China where the rockets were used to start a fire. Development of rockets and their military use kept continuing in the direction of longer range and higher capacity. It was noted that in the 17th and 18th century thousands of iron rockets had been used exclusively in battles.

Unlike its baby steps in middle age, the modern-day ballistic missiles roots lie in World War II where V1 and V2 ballistic missiles were launched by Germany during 1944 - 1945. The first V1 was dropped on June 13, 1944 and the last one on March 27, 1945 causing thousands of casualties. During that time the 2nd iteration of this so called "vengeance weapons" German V2, the precursor of modern-day missiles which was propelled by a single stage fuel following a ballistic trajectory fired against Britain in September, 1944. V2 missiles were less accurate as compared to V1 missiles. Countermeasures against this supersonic, gyro-guided missile which was equip with approximately 900kg warhead was extremely difficult. Since they were travelling faster than the speed of sound and making no warning sound before crashing down it was almost impossible to defend against. On the other hand, the result of a successful V2 hit was devastating.

Ever since V2 took place in military scene, the studies of missile technology accelerated. V2's propulsion and guidance problems along with defense against ballistic missiles had been studied increasingly. By the end of the World War II, several countries were working on similar technologies. Unfortunately, Turkey was not able to contribute to those studies at that time.

However, with the advent of Cold War, Turkey took place in missile scene indirectly. The United States placed several nuclear ballistic missiles in 1959 that would be removed later on[1]. Apparently developed countries use missiles to enhance their deterrence.

Since the primary objective of Turkey is to protect and preserve its independence and territorial integrity, having missiles serves as an insurance policy preventing possible international tensions. It should be also noted that having missiles in a country arsenal is

not enough. The more important part is to have that technology and develop those missiles singlehandedly.

Over the last 30 years, Presidency of Defense Industries has made incredible progress in building Turkey's modern national defense industry. Today over 600 defense projects total of 76 billion USD is being caried out in Turkey. In 2024, another notable progress is to have the rate of national domestic participation to reach the level of 80%. This goal leads to significant research and development investments in a locally produced projects.

Aim of this thesis is to design of folding tail fin which would be used in locally developed long-range high-altitude air defense missile. The present study relates to deployment mechanism used in the subsystem of the missile. Main objective is to design and analysis the mechanism, then validates its performance by number of tests. Lastly, all the parts in abovementioned system shall be locally manufactured so that the final product could be used in domestic air defense systems.

This thesis is composed of five chapters. In Chapter 2, literature review is presented. In Chapter 3, the fundamental design concept shall be demonstrated. In Chapter 4, the outputs of the study are discussed. In the last chapter, this thesis concluded with the contribution of said mechanism.

2. LITERATURE REVIEW

Missiles are guided ranged weapons propelled by rocket motor according to military terminology. Although missiles and rockets are generally used synonymously, the difference between missiles sand rockets is missiles have guidance system. After missiles are fired, their trajectory could be maneuvered during flight. Almost all missiles have some form of guidance system therefore they are also known as guided missiles. In military usage, a missile always refers a guided munition. On the other hand, an unguided missile is defined as rocket. A rocket trajectory is based upon how much propellant is available and the elevation angle of the rocket launcher. After the launch there is no way to change the trajectory of the rocket. This type of flight is called ballistic flight and it is based on ballistic flight equations.

As abovementioned missiles have a number of different subsystem components such as guidance system, targeting system, flight system, engine, warhead etc.

Classification of missiles could be based upon subsystem such as guidance system and many more. In the following section different classification types will be explained.

2.1. Classification of Missiles

2.1.1. Based on Guidance

2.1.1.1. Command Guidance

In this guidance method, guidance commands are generated apart from the missile. Generally, these commands are calculated by a guidance processor based in the missile launch area and transferred to the missile. Radars follow the target and missile then provide the necessary data to computer to carry out necessary guidance commands. After that these commands transferred to the missile.

2.1.1.2. Homing Guidance

Homing guidance represents a missile which contains a seeker. Seeker sees the target and feedbacks guidance to calculate possible interceptions with target. Also, the homing missile can be divided into subsystems such as active, semiactive and passive guidance systems.

2.1.1.3. Beam Rider Guidance

A guidance system that constrains guidance to a beam. Beam is created by a radar which illuminates the target. While missile stays in beam, it will move towards the target.

2.1.1.4. Inertial Navigation Guidance

An inertial navigation system is a self-contained navigation method where data provided by accelerometers and gyroscopes to track the position and orientation of an object whose starting point, orientation and velocity are known. Gyroscopes provides turning rate measurements. Accelerometers provides change in the velocity. Inertial navigation guidance continuously calculates the position, velocity and acceleration of the missile then provides navigation guidance without the need for communication via ground station.

2.1.2. Based on Method of Launching

Although vast variety of missile types exist, most common ones based on launching method are explained in this section. (Marine types are not mentioned.)

2.1.2.1. Surface to Surface Missiles

Surface to Surface Missiles (SSM) are the common ground to ground missiles. They can be either used as an offensive long-range weapon or to support ground troops as an artillery battery. Their maneuverability is very low. Because of this reason they are launched upright position.

2.1.2.2. Surface to Air Missiles

Surface to Air Missiles (SAM) are the main element of an area defense system against aircrafts or other hostile missiles. Their design range can vary from a few miles to several hundred miles depending on the threats. Generally, a single stage solid rocket motor is preferred for short ranges. For longer ranges, multistage rocket motors are required.

2.1.2.3. Air to Air Missiles

Air to Air (AAM) missiles are used for airborne battles. These are mounted under the fuselage of aircrafts or unmanned aerial vehicles. The maneuverability requirements of AAMs are the most demanding as compared to the other missile types.

2.1.2.4. Air to Surface Missiles

Air to Surface Missiles (ASM) are used as a tactical weapon to knock enemy ground targets out. Most of the ASMs are designed as fire and forget from standoff distance which means that ASMs can be launch from aircrafts from a distance without coming within range of the hostile air defense zone. A frequently used ASM is cruise missiles which are capable of travelling long distances at high speeds while autonomously finding the enemy target.

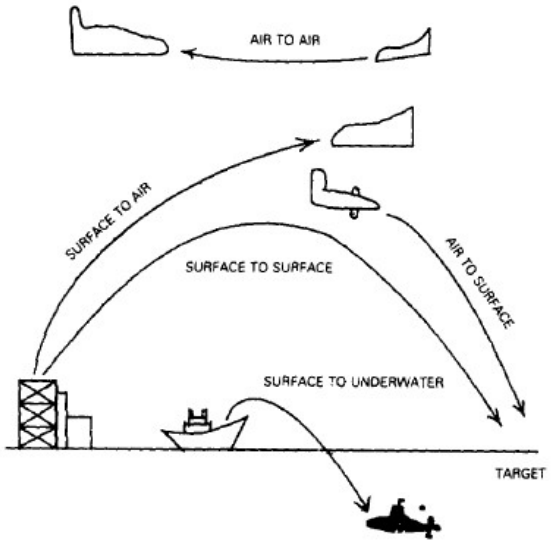

Figure 1 Missile Classification by Method of Launching[2]

2.1.3. Based on Range

On the basis of range, SAMs are broadly classified as follows;

2.1.3.1. Short Range Surface to Air Missiles

Short range surface to air missiles (SRSAMs) which travel up to 30km are called short range missiles. They are used for point defense against helicopters and low flying aircrafts.

2.1.3.2. Medium Range Surface to Air Missiles

Medium range surface to air missiles (MRSAMs) have a range between 30km to 100km. They are generally used for tactical aircrafts and unmanned aerial vehicles (UAVs).

2.1.3.3. Long Range Surface to Air Missiles

Long range surface to air missiles (LRSAMs) have a range between 100km to 400km. They are primary defense system against high altitude threats but lack defense against

intercontinental ballistic missiles (ICBMs). Since ICBMs can travel more than 5000+ km at very high speeds often reaching hypersonic velocities and they fly at high altitudes typically above 100km, the reaction window for interceptors is very short in order that extended range surface to air missiles (ERSAMs) with 400+ km range are used to increase the interception possibility.

2.1.4. Based on Aerodynamic Control

Further differentiation among missiles can be made on the basis of aerodynamic control.

2.1.4.1. Wing Controlled

A wing control consists of relatively large wings attached close to the center of gravity (Cg) of the missile and set of tails at the aft section.

2.1.4.2. Canard Controlled

A canard control consists of small control surfaces located at the front of the missile and set of large wings or tails attached to middle or aft section.

2.1.4.3. Tail Controlled

Tail control refers to the use of control surfaces attached at the rear of a missile.

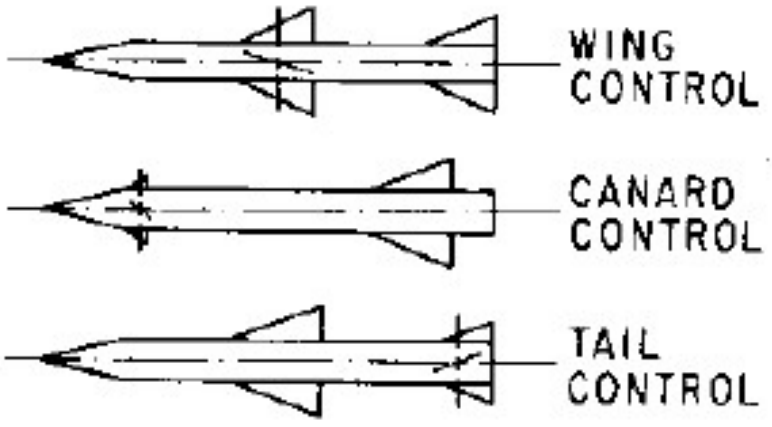

Figure 2 Types of Control Configurations[3]

The missile mentioned in this thesis is a long-range high-altitude surface to air missile. Since the said system is long range, it uses multistage solid propellant rocket motor (SRM). In the very beginning of the flight, a droppable booster motor gives a short burst of power. When the booster burns out, it is separated from the missile. After that dual pulse motor, mounted in tandem layout, is ignited.

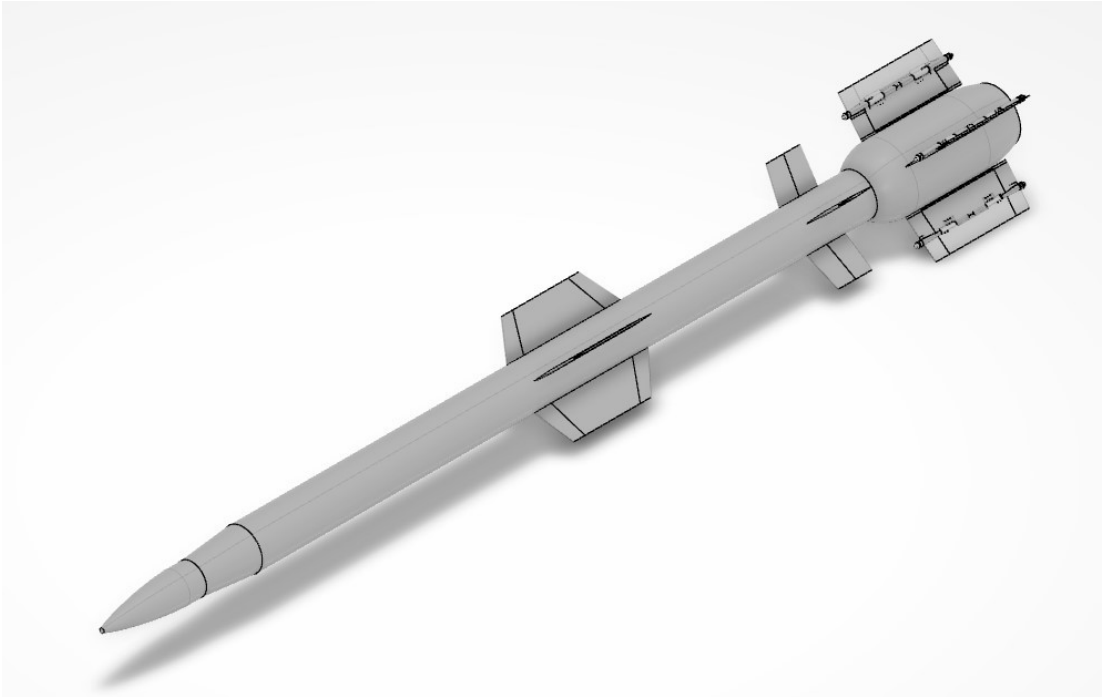

Figure 3 Isometric View of the Missile

It was a necessity to compose proper subsystems on hand and develop new systems if there is none.

For abovementioned missile, it is mandatory to develop folding tail fins located on booster motor. The necessity of folding mechanism is not a new challenge. Different mechanisms have been studied for decades for different types of missiles by flagships of defense industry companies. However domestic design and production has yet to be done locally for such a missile.

For this thesis, a comprehensive investigation of used mechanism was carried out. Conducted patents were studied. In the next section types of different folding mechanisms shall be demonstrated.

2.2. Classification of Folding Mechanisms

2.2.1. Bendable/Flexible Members

A folding method of an air vehicle wings was explained in this patent[4]. Air vehicle includes a fuselage and wing connected to the fuselage. Wings are wrapped around the fuselage to decrease the space occupied.

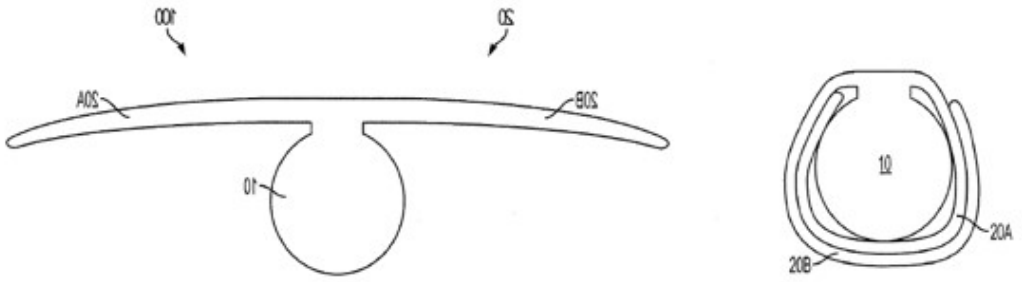

Figure 4 Bendable/Flexible Wings[4]

According to patent holder this invention is not limited to air vehicles but also it could be applied to any system with bendable or flexible members. However, it is suggested that the member should be made of fiberglass or carbon fiber. Additionally, the connection between fuselage and wings could be permanent, temporary or adjustable based on molding process.

After the wrap around, the air vehicle is placed in the storage container. The integration could be either tight or loose. According to the intention, looser fit may ensure it release upon leaving the constrained volume allowing to unfold smoothly.

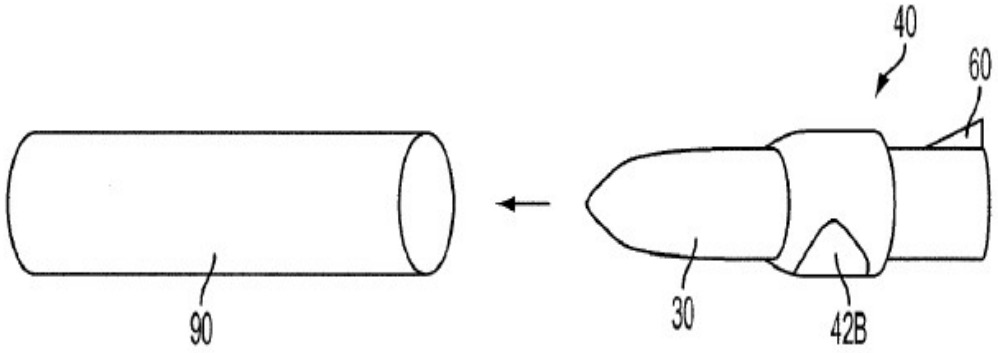

Figure 5 Integration of Bendable System[4]

This patent claims that it solves poor flight performance caused by short wingspan. This solution could increase wingspan substantial amount and it might be a good solution for unmanned air vehicle or manpad systems.

2.2.2. Motor Driven Mechanisms

This patent[5] describes a discrete extendable wing mechanism unit assembled into guided airborne body. The mechanism comprises a driving motor, lead screw which is driven by motor, extendible pair of wings pivotally coupled to the carriage and other mechanical elements. It is claimed that by the motor drive forward and rear wings move between stowed position and deployed position. One of the advantages of this mechanism is that the position of the wings could be arranged according to mission profile requirements. Wings could be fully extended state or partially extended or even it could be retracted back in order to control lift and drag force. Another advantage is diamond shape extended wings produces aerodynamically balanced high lift drag ratio.

This separate kit could be attached to guided airborne, missiles, inertially aided free fall weapons, munitions, rockets etc. to provide control and extended range capacity. Major advantage of this mechanism is its simplicity and low-cost installation on existing systems.

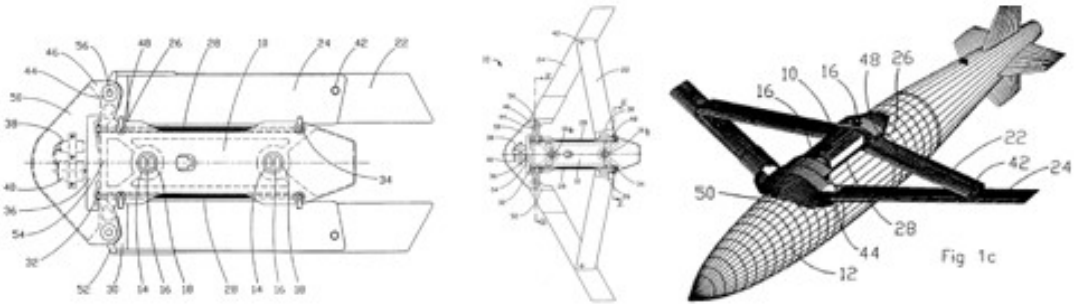

Figure 6 Extendable Wing Mechanism[5]

2.2.3. Spring Powered Mechanisms

European patent EP3165870A1[6] describes spring powered folding wing for a missile. It comprises wing root, wing body prestressed force element and latching mechanism. This patent does not contain any electronic components but only simple mechanical robust parts.

By using prestressed spring which introduce torque around the swiveling axis, after launch of the missile upon releasing from the storage, wings shall unfold permanently to flight position.

Another spring element, it could be either tension or compression spring depending on the design, is used in the latching mechanism in order to hold the wing body permanently locked on the flight position. Second prestressed force element axially secures the wing body to the wing root after rotation is complete.

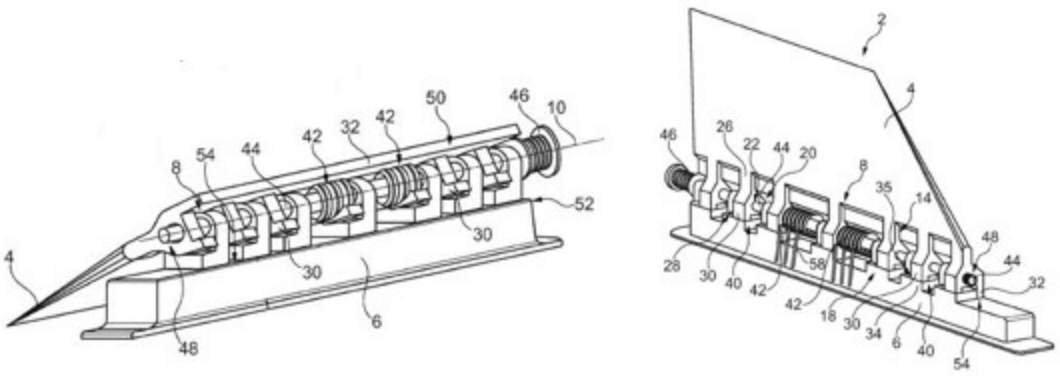

Figure 7 Torsion Spring Mechanism[6]

Major advantage of this system is that it is simple and reliable. However, this system is suitable for small wings with short wingspan. As the inertia of the wing along with wing span increases, higher torque requirement is necessary which may not be possible with simple torsion springs. For high torque applications there are different solutions in literature. Additionally, it is important to note that swivel axis should be in the vicinity of the wing root in the mechanism shown above.

Another spring powered patent[7] relates to a latching mechanism of a folding missile wings. It was claimed that it comprises a rotable hub, a bolt which is loaded by a compressive spring and slides in said hub, lastly control surfaces and hinge body. It is understood from the patent that inventor refers control surfaces by saying wings which are movable steering elements. The difference is, control surfaces are pivotally controlled during flight and they are not stationary.

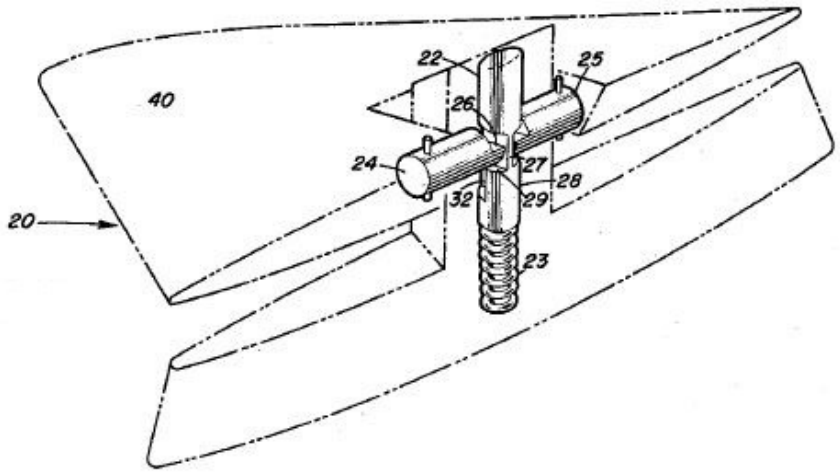

Figure 8 Latching Mechanism of a Folding Missile Wings[7]

Spring powered systems might be the most common mechanism used in folding applications. This patent[8] is an ingenious use showing a flip out wing mechanism where compressive spring urges plungers rearwardly toward their lock position. End surface of the plunger is arcuate. When the spring extends, the lug of the wing rides on the arcuate end portion of plunger. When spring is fully extended, the lips and the recess interengage that prevents inward movement.

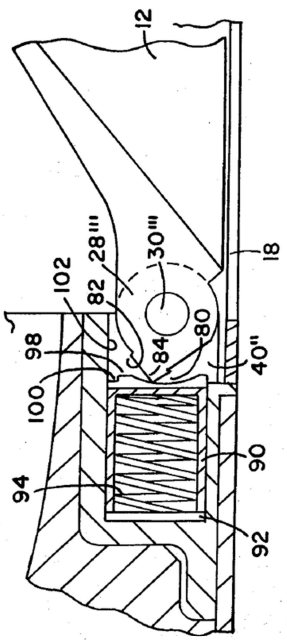

Figure 9 Arcuate Plunger Driven by Compression Spring[8]

Another humble yet effective mechanism, sliding fin lock was introduced in this patent[9]. Inventor claims that it is simple and inexpensive mechanism consists of easy to manufacture minimal number of elements. Core parts of the mechanism contains two sliding locks, two fin lugs, a compression spring and a hinge pin. Upon deployment, compression springs moves sliding locks against the fin lugs so that the protruding and recess surfaces engage. The contact area is horizontal plane surface however it was suggested that it can be manufactured as an inclined surface to produce a wedging effect.

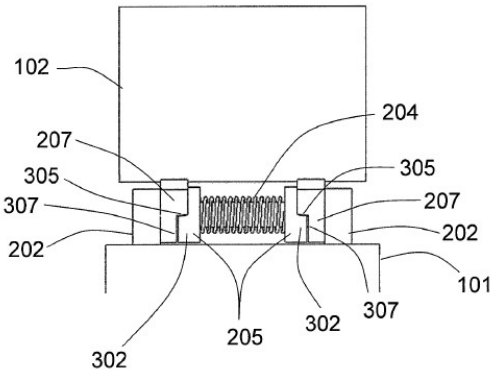

Figure 10 Dual Sliding Fin Lock Mechanism[9]

Most spring-based designs focus on using compression springs because of its inherit design and integration advantages. They contain limited number of parts which are easy to manufacture and assembly. Additionally, it turns out to be more reliable mechanism. It can be used for repeated cycles without failure.

However, there are designs utilizing tension springs such the following patent.

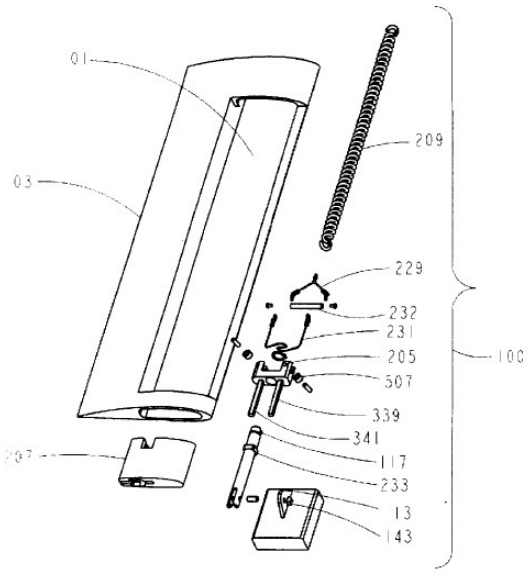

Figure 11 Tension Spring Mechanism[10]

Unlike compressive springs, this mechanism has wide range of parts such as Kevlar ropes in Y and U-shaped geometry, swivel, shaft, base part, and bushings. It is also stated that it requires adhesive bonding between wing and base plate. As compared to compressive spring designs, this mechanism is quite complex and the reliability of the mechanism depends heavily on process that is why it is considered less reliable option.

2.2.4. Pneumatic/Hydraulic Powered Mechanisms

Another interesting design concept of cam following folding wing mechanism was demonstrated in this patent[11]. A slidable shaft actuated by pneumatic or hydraulic power (compressed air stored in the form of an explosive cap or high-pressure fluid) makes the cam follower on the wing follow predetermined path. By changing grooves one can alter the kinematic motion of the wing. Alternatively, designer can achieve acceleration slope in the beginning and deceleration slope before erected position in order to prevent wings from being broken off as they hit their rest position. Additionally, it helps movement without excessive vibration and shock.

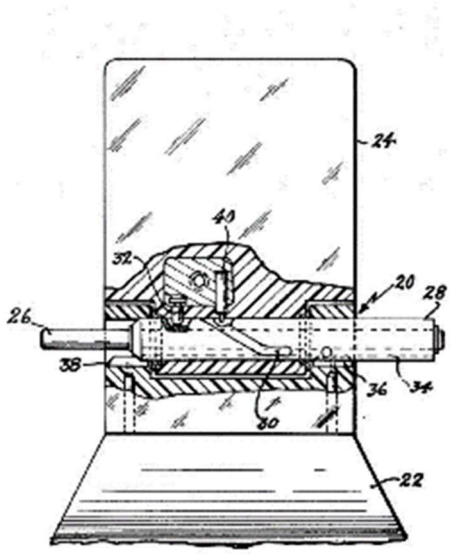

Figure 12 Cam Follower Mechanism[11]

It is not very common to use pneumatic actuators in folding mechanism however it has some applications like above. On the other hand, one orthodox invention which pertains by means of gas pressure springs suggested here[12]. Gas pressure spring can be linked to the lower and upper wing parts at a rather high effective lever arm. It unfolds wing in a completely automated fashion just after the takeoff. After completion of deployment, gas pressure spring can be jettisoned under assistance of an auxiliary spring.

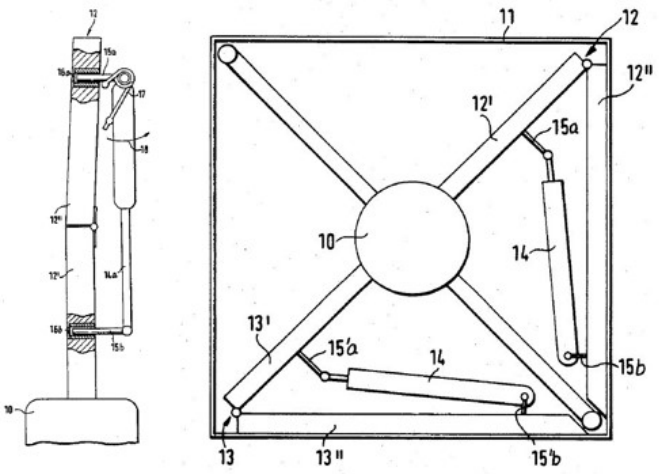

Figure 13 Gas Pressure Spring[12]

2.2.5. Double Swing Self Erecting Mechanisms

This patent[13] shows worm gears assembly which transmit rotary movement to a turntable. Turntable is also turnable on base member itself. The rotation of the wing is affected by drag force and inertia of the accelerating missile. Optionally it can be powered by actuator which is not shown in figure.

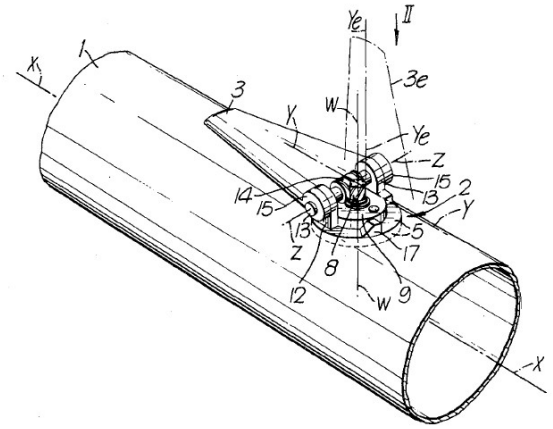

Figure 14 Turntable Folding Fin Mechanism[13]

A simpler invention for small wings utilizing annular shaped clevis is explained in this patent[14]. The clevis is attached to missile fuselage and hinged to the lug of the wing at a 45° angle.

This mechanism rotates upwardly from the horizontal stowed position into vertical position also known as feathered position. The wing is stowed along the side of the missile in horizontal plane. When deployed, it rotates upwardly into vertical plane.

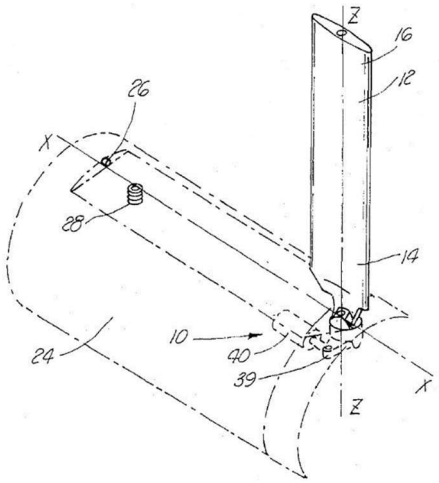

Figure 15 Missile Appendage Deployment Mechanism[14]

Similar approach was applied to the following patent[15]. This guided anti-armor missile wing also both rotates about its spanwise axis relative to an erected position and pivoted forward alongside the air frame. The wing includes a secondary wing within the wing itself in which passing air enables wing surface to automatically deploy so that it increases surface area.

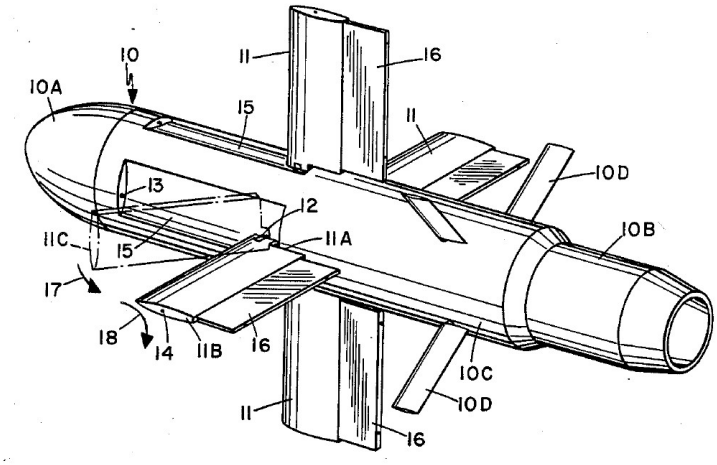

Figure 16 Self Erecting Wing[15]

This mechanism has some interesting features that should be noted. First one is that the wing is shaped and dimensioned so that in retracted position it conformally stored in the recess of the fuselage. This solution enables to be able to launch the missile from a tube conforms to the shape of the missile air frame.

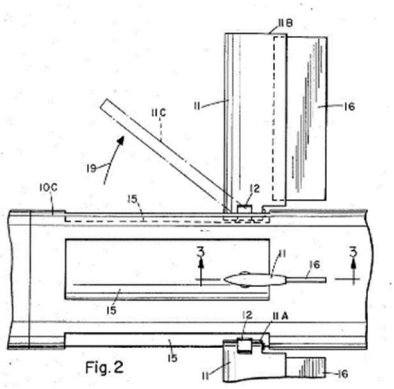

Figure 17 Conformal Wing Geometry[15]

Second one is the retainer which contains a solenoid, spring and tip. By energizing the solenoid, the tip is withdrawn and wings can pop out.

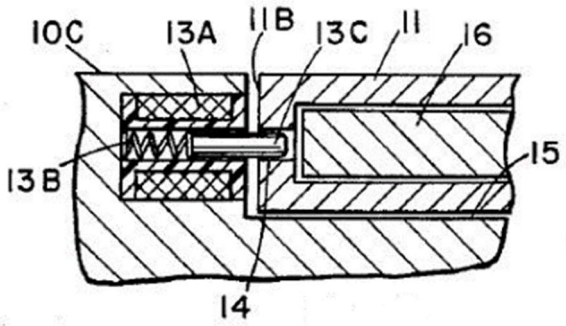

Figure 18 Solenoid Retainer Mechanism[15]

Third one is the locking mechanism. Once the wing is fully erected, a trunnion lock prevents further rotation. Trunnion lock contains spring, pin and hole. Pin is guided along the groove until recess. When pin reaches the recess, spring pin hole combination gets stuck. This solution is quite simple yet effective that is the reason it was considered to be used in the system subjected to this thesis.

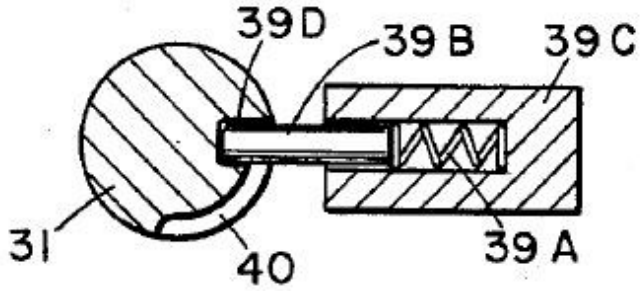

Figure 19 Trunnion Lock[15]

2.2.6. Pyrotechnic Driven Mechanism

This invention[16] describes a pyrotechnic driven folding mechanism. It is a fast, non-retractable solution dependent on overcenter action. Wings are stored in folded condition by pyrotechnic actuator. When the pyrotechnic actuator is ignited, it generates high pressure fluid against an actuator piston. This piston drives overcenter mechanism which deploys and locks wing in the extended position.

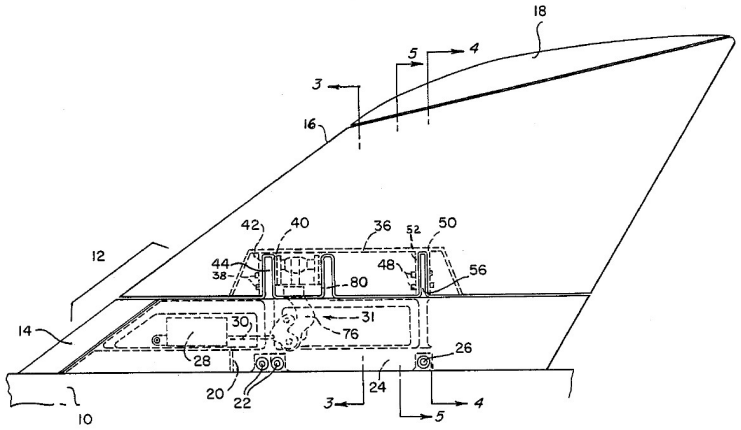

Figure 20 Pyrotechnic Driven Mechanism[16]

2.2.7. Torsion Bar Mechanisms

A deployable wing mechanism, unfold by a torsion bar explained in this patent[17]. Mechanism contains hollow shaft where the torsion bar is located. Torsion bar is fixed at the end to the pod and fixed at the end to the inner part. When the wing is released from its folded position, torsion bar forces wing back to its deployed position.

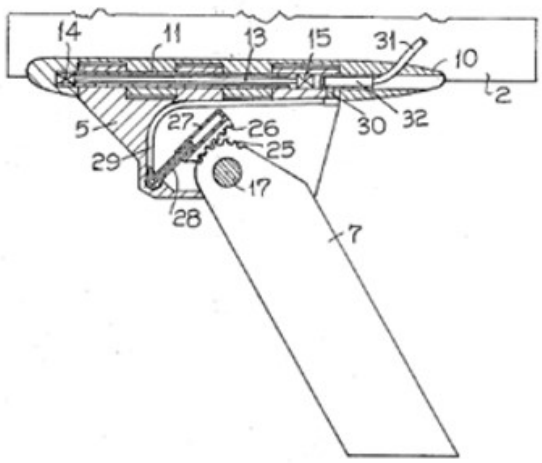

Figure 21 Torsion Bar Mechanism[17]

This patent[18], folding wing configuration utilizing double torsion bars. A solid torsion bar positioned within a hollow cylindrical torsion bar concentrically. Both torsion bars lie longitudinally along inboard wing section. By folding the hinged wings into the storage condition, springs stores potential energy which will be later used to drive overcenter deployment linkage through gear train for deployment.

Placing torsion bar longitudinally inside the wing aerofoil is an ingenious space usage which utilizes chord length effectively. Similar analogy shall be used in our system.

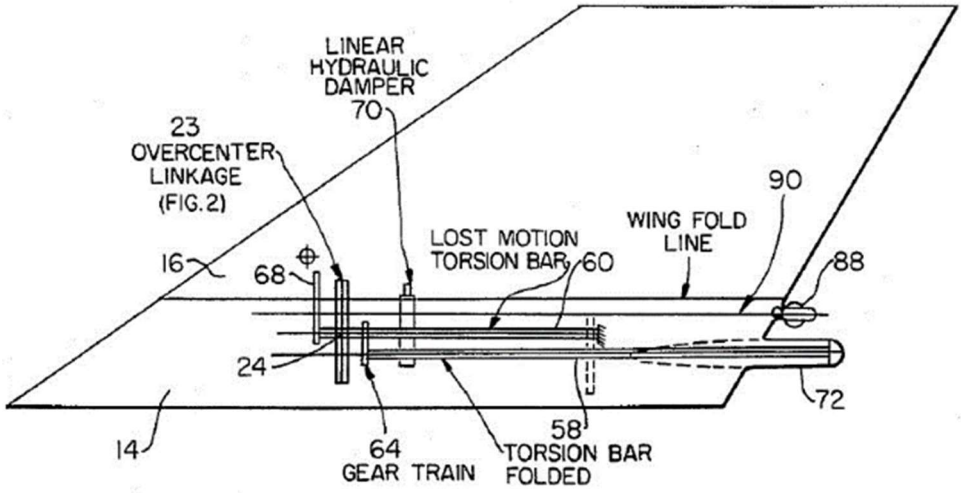

Figure 22 Double Torsion Bar Longitudinal Mechanism[18]

2.2.8. Leaf Spring Mechanisms

This section is dedicated to leaf spring mechanisms. It is not a repetition of section 2.2.3 but leaf spring designs are considered to be mentioned as a new section.

This patent[19] shows a folding wing mechanism actuated by leaf springs. Base part of the mechanism is rigidly fastened by using welding on the missile body. There are compound leaf springs located inside the base part on a V shaped notch profile. The end part of the longest leaf spring interacts with movable inserts. The upper part of the wing is pivotally connected to movable inserts which could only move in horizontal direction. By moving movable inserts upwards, leaf springs stores potential energy. Upon release of the folded wing, springs return to their free position while rotating the upper body.

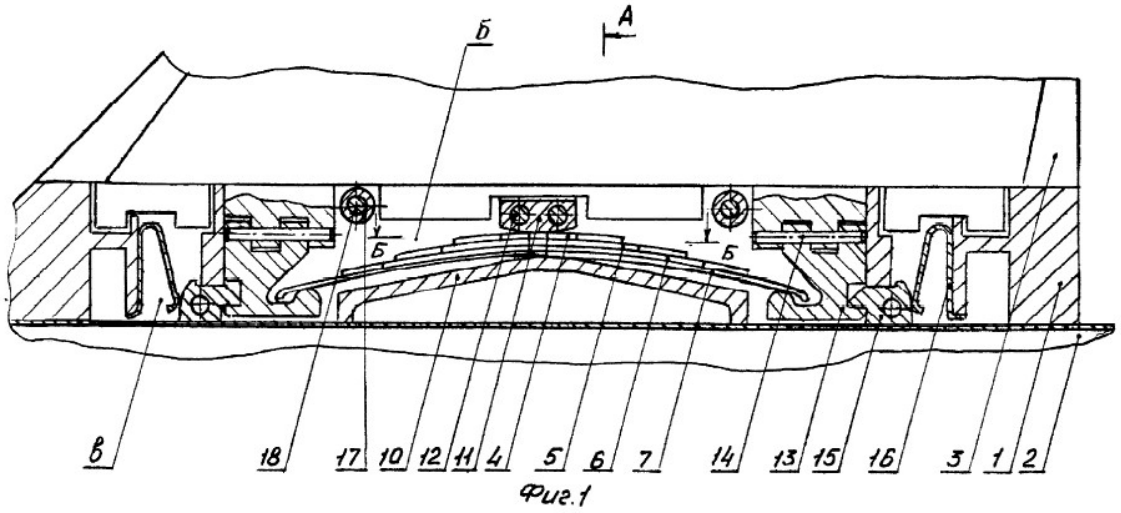

Figure 23 Leaf Spring Folding Mechanism[19]

After deployment, the movable inserts are locked by fixation element. Fixation element which is a flat clamp is pushed against the recess part of the movable inserts and gets locked.

There is similar leaf spring powered folding mechanism designs in the literature with minor differences on their fixation mechanism such as the following patent.

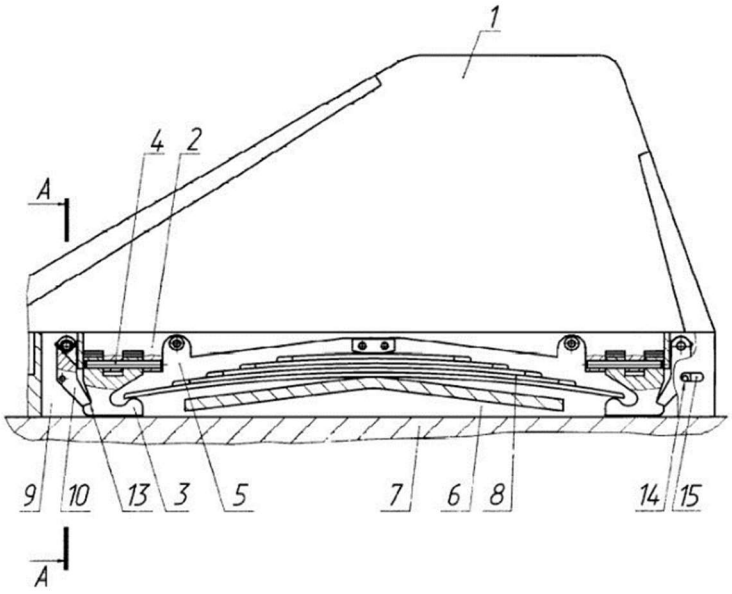

Figure 24 Leaf Spring Design with Different Fixation Element[20]

According to the inventor, object of the newer design is to eliminate locking problems experienced with the original flat clamp fixation element. It is claimed that the newer invention reduce friction substantially so that it eliminates possible jamming and misalignment problems.

2.2.9. Miscellaneous Systems

This patent[21] shows a deployment mechanism for missiles launched from internal bays of aircrafts. It is an apparatus rather than a mechanism that employes cam tracks and track follower pins in a totally passive fashion. A plate with a cam track on it is fixed on aircraft body. The opposing male part which is track follower pins are located on the rear part of the folded wings. As the missile is ejected in the direction of gravity vector, fins move through predetermined slots. Meanwhile two of the folded wings shall deploy.

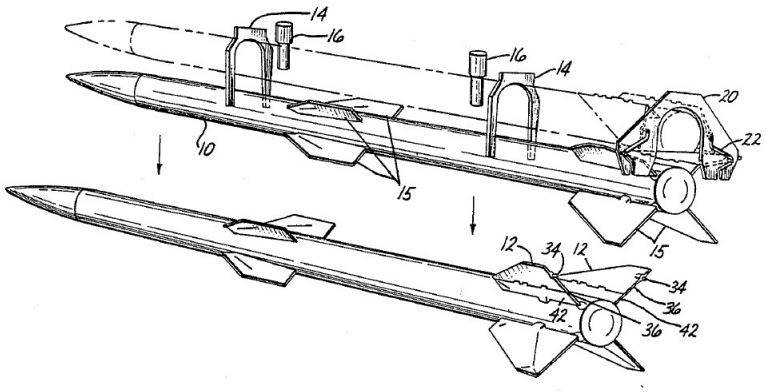

Figure 25 A Passive Deployment Apparatus[21]

Following patent[22] is a deployment mechanism which engages fins mounted in the central region of the missile tail. This invention consists of a scotch yoke mechanism sliding axially on a shaft, driven by a compression spring. When compression spring is released, the scotch yoke mechanism pushes against the inwardly facing, pivotally mounted tail fins; causing tail fins to rotate from stowed position to the erected position.

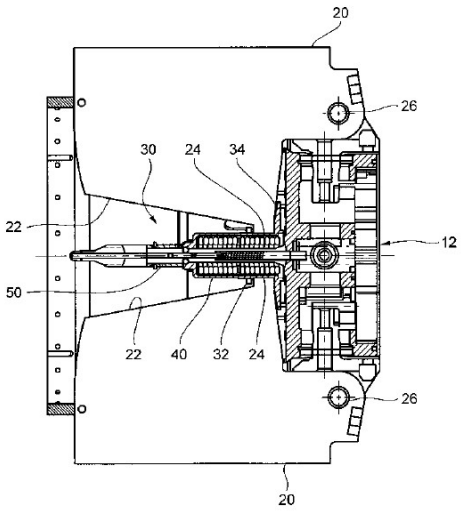

Figure 26 A Scotch Yoke Deployment Device[22]

3. MATERIAL AND METHOD

Guided missiles are stored in missile canisters during storage, handling and transit stage up to missiles are being fired. A missile spends most of its time in canister as compared to the other product life cycle stages. Hence a missile canister plays an important criterion in the design of a missile in the first place. In system design perspective, the design requirements of the missile are defined beforehand and assigned itself in predesign stage. Due to space, weight, transportation, launch cell limitations etc. it is not possible to increase dimensions of missile canisters as designers wish. Most of the time canisters are tightly packaged. Because of this reason, missile packaging is directly affected by canister dimensions too. Since the missile extremities are imposed by tail span; It is necessary to fold those parts to fit into canisters in a stowed position while decreasing the space occupied. Folded tail fins in our cases needs a mechanism to hold tail fins as close to the fuselage as possible upon release and then serves as a deployment mechanism to lock fins into their fully opened position.

Design study starts with defining canister inner dimensions and possible maximum wingspan. In a CAD platform preliminary design had been carried out and maximum of 230mm wingspan folding at 130mm from root was decided in the first place.

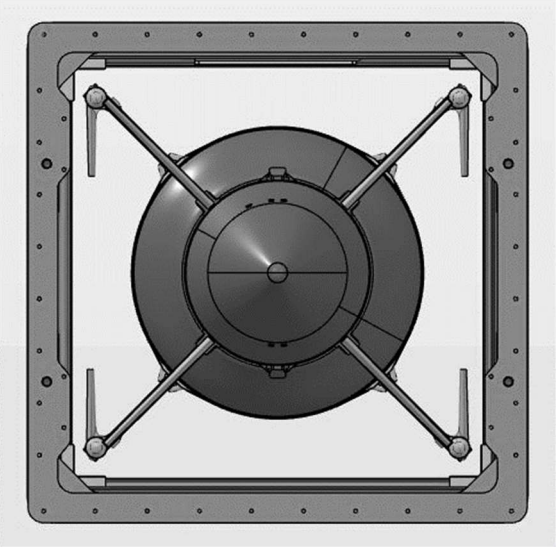

Figure 27 Folded Tail Fins View in Canister

Remembering that most of the folding mechanism focus on folding wing at root, it was a challenge to fold wing from the middle section. In order that, the longitudinal chord length must be used effectively. Because of this reason a torsion spring laying parallel to the longitudinal axis was considered to be used.

All conceptual and detail design is carried out in Catia 3D modeling platform. Modeling and packaging requirements are assigned from canister needs. According to those requirements preliminary spring calculations had been carried out analytically. Difference between regular torsion spring and square shaped torsion spring will be shared in the related part.

According to preliminary design parameter such as deployment time, safety factor of torsion spring and physical packaging of folding tail fin, conceptual design of folding tail fin was conducted.

Since this thesis consists of design, analysis and manufacturing parts, all stages are confirmed with validation tests. Additionally, special test fixtures and test apparatuses were designed and manufactured for every stage; totaling of 4 different test fixtures and 2 different test apparatus.

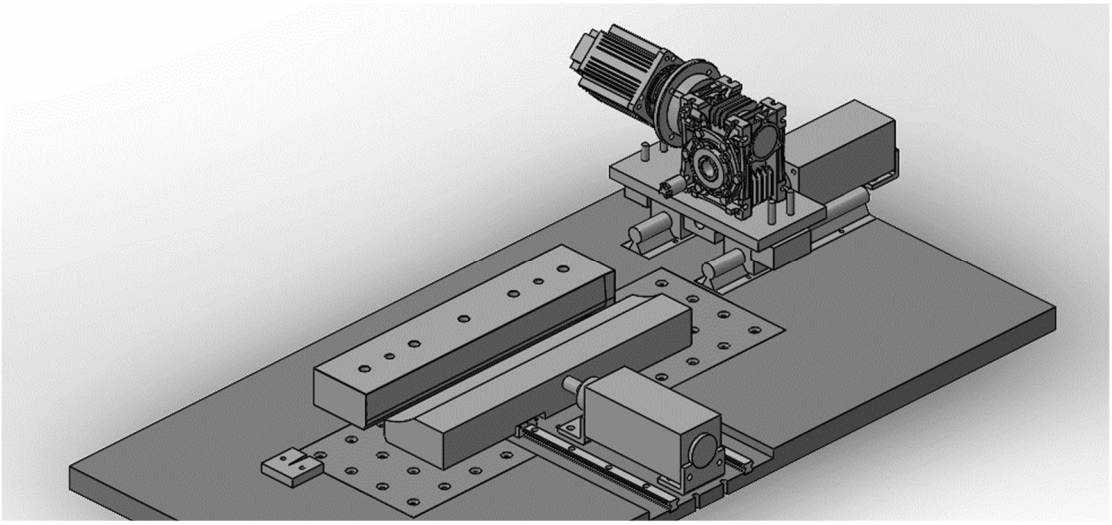

Figure 28 Design of Folding Tail Fin Deployment Test Fixture

Details of fixture and apparatuses process shall be unrevealed. However, in every related part, detailed pictures are given.

In this thesis, 3 different types of analysis are performed. Firstly, aerodynamical analysis is carried out in Ansys Fluent. After that fluid to solid interface analysis is performed in Ansys Structural. This is a single-iteration aeroelastic analysis of the airfoil body.

Following this series of analysis, they are enriched by fatigue analysis of torsion spring and dynamic analysis of folding tail fin. Ansys analysis tools are used for complete range of analysis except that dynamic analysis is performed on MSC Adams.

4. RESULTS AND DISCUSSION

4.1. Analytical Calculations

4.1.1. Calculation of Torsion Spring

It is required to produce most torque in the smallest area possible so that calculation had started with torsion spring then for higher spring constant, square shaped helical torsion spring is decided to use.

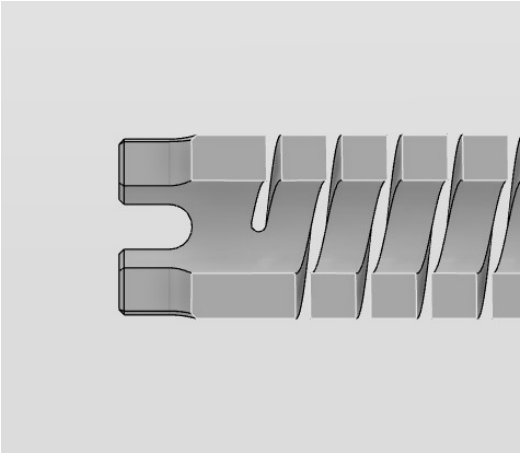

Figure 29 Cross Section of Square Shaped Torsion Spring

The spring rate k in torque per radian in torsion springs is given by

$$k = \frac{d^4 E}{64DN} \tag{4.1}$$

where D represents coil average diameter and N represents number of active coils.

Not also design limits, but also manufacturing process plays an important role for producing square shaped helical torsion spring. It is most commonly produced by EDM process which requires a pilot hole beforehand. Pilot hole is directly affected by part length.

Additionally decreasing part length also increases spring constant while decreasing safety factor of the spring.

Main objective of deciding proper spring parameters is to have highest available spring constant while being safely under the yield strength.

Stress induced on the torsion spring upon loading is given by

$$\sigma = \frac{6T}{d^3} \tag{4.2}$$

Square cross section helical torsion springs have higher energy storage capacities than regular torsion springs.

The spring rate for square cross section torsion spring is:

$$k = \frac{d^4 E}{41.45DN} \tag{4.3}$$

Material was chosen 17-4PH H1025. Young Modulus of 17-4PH is 196.5 GPa. We find analytically that for our chosen design parameters d, D and N, spring constant is;

$k = 3.025$ Nm/rad

Since torque equation is given as;

$$T = -k\theta \tag{4.4}$$

Square cross section helical torsion springs have higher torque inherently as compared to regular torsion springs that is why this spring is chosen for our application.

With an angular displacement of 135°; by using equation (4.2) and yield strength of 1000 MPa, factor of safety of 2.05 is calculated for the abovementioned spring.

For known torque and angular displacement, one can calculate spring rate. In order to calculate spring rate, a test apparatus was designed. Test apparatus is a hollow cylinder which is used to hold torsion spring still at the bottom end while allowing to apply torque from the top end.

Figure 30 Spring Rate Test Fixture

For different angles, corresponding torque value can be read from electronic torquemeter. Calibration of digital torque meter was already done beforehand.

Spring rate is simply calculated from equation (4.4).

Figure 31 Torque Reading

Single folding tail fin consists of two torsion springs embedded in airfoil body. They are working in parallel. Total spring constant is given as,

$$k_{eq} = k_1 + k_2 \tag{4.5}$$

A test had been conducted to obtain spring rates. By using test apparatus, torque values at different angles were found for two torsion spring specimens.

Table 1 Spring Constant Test Matrix

Angle (rad)	**Torque of torsion spring #1 (Nm)**	**Torque of torsion spring #2 (Nm)**
0.17	0.63	0.68
0.35	1.11	1.14
0.52	1.62	1.83
0.70	2.10	2.36
0.87	2.66	2.88
1.05	3.28	3.33
1.22	3.74	3.78
1.40	4.36	4.36
1.57	4.81	4.87
1.75	5.34	5.41
1.92	5.78	5.92
2.09	6.18	6.27
2.27	6.67	6.79
2.44	7.38	7.36
2.62	7.74	7.88
2.79	8.37	8.21
2.97	9.13	9.01

Test results of each spring are represented graphically below.

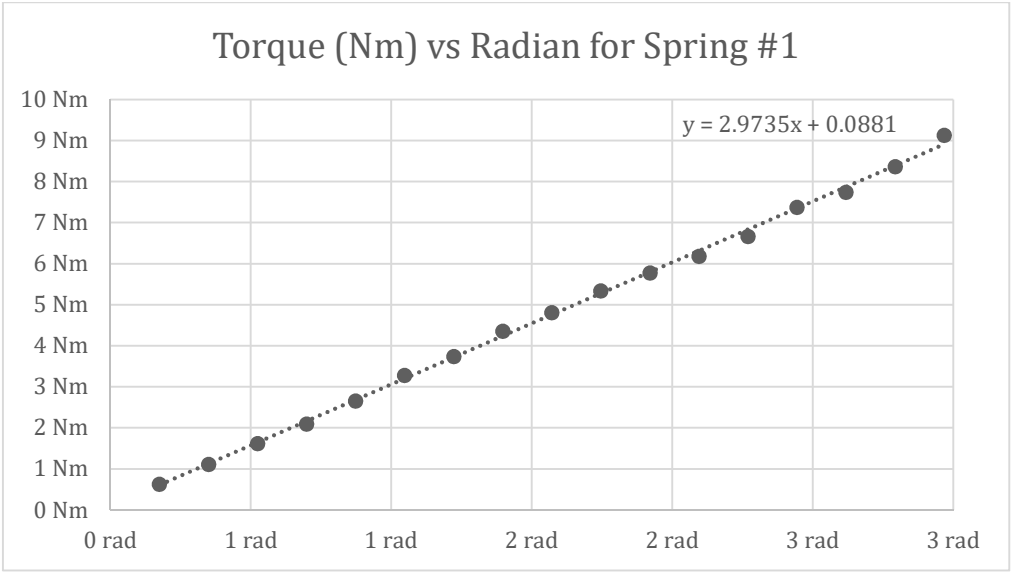

Figure 32 Spring #1 Test Result

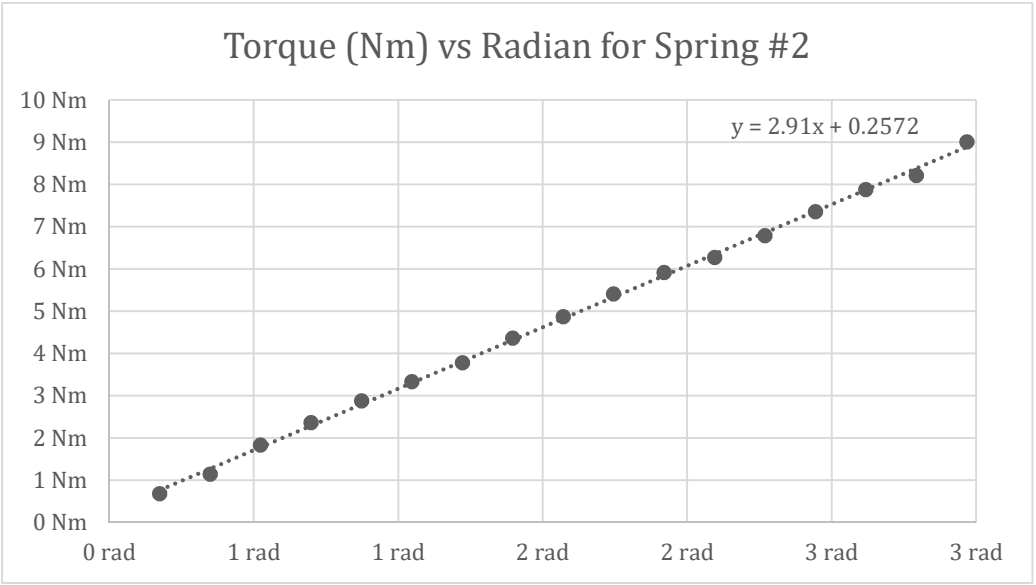

Figure 33 Spring #2 Test Result

Slope of the trendline gives the rate of change of torque value over angular displacement, simply the spring constant of torsion spring where there is a linear relation as eqn. (4.4) suggested. The equivalent spring constant is calculated by summation of each spring as;

$k_{eq} = 5.88$ Nm/rad

The manufactured springs yielded consistent results. As compared to analytical calculation, there is only %3 deviation which indicates we are able to properly produce springs according to our design parameters.

4.1.2. Calculation of Deployment Time

As previously stated, deployable folding tail fins located on booster motor. Since booster motor runs very short duration of time, the deployment time window for tail fins is even shorter. It was assigned as the maximum deployment time should be less than 100ms to the tails.

Even though folding tail fin has 2 different body, the lower part is stationary. Only the upper part rotates around the rotation axis as can be seen below.

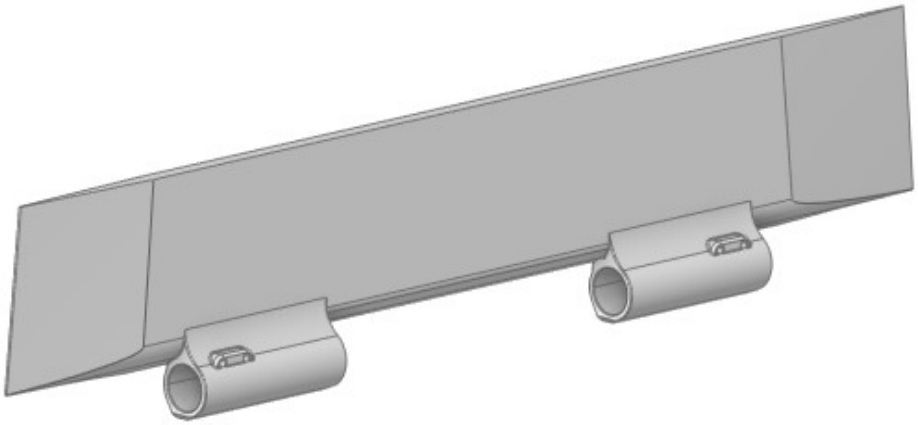

Figure 34 Rotating Body of the Folding Tail Fin

Moment of inertia of the upper body w.r.t the chosen axis of rotation is $I = 0.004\ kgm^2$

Work kinetic energy theorem is extremely useful in describing the motion of the body. Work done by external forces equals the change in the rotational energy.

$$\sum W = \int_{\theta_i}^{\theta_f} \sum \tau \, d\theta = \int_{\omega_i}^{\omega_f} I\, \omega d\omega = \frac{1}{2} I\omega_f^2 - \frac{1}{2} I\omega_i^2 \tag{4.6}$$

Substituting the total torque from Eq. 4.4 and integrating gives

$$\frac{1}{2} k\theta_i^2 - \frac{1}{2} k\theta_f^2 = \frac{1}{2} I\omega_f^2 - \frac{1}{2} I\omega_i^2 \tag{4.7}$$

Where the angular velocity changes from 0 to ω_f as the angular position changes from θ_i, folding angle, to 0. After that for every angular position, the corresponding time step could be calculated. Summation of these time steps give the total deployment time.

Table 2 Input Parameters for Deployment Time

k_{eq}	5.88	Nm/rad
I	0.004	kgm^2
Folding Angle	2.35	rad

Total time has been divided into 0.017rad subintervals of equal size. Calculation of each interval and summation of them as total deployment time are shared at appendix A.

Total time is calculated as 39ms for 2.35rad folding angle. Now that we have satisfactory analytical solutions for both spring rate and deployment time, it is better to design tail fins in details while conducting necessary analysis. A predesign of folding tail body is depicted in Fig. 35.

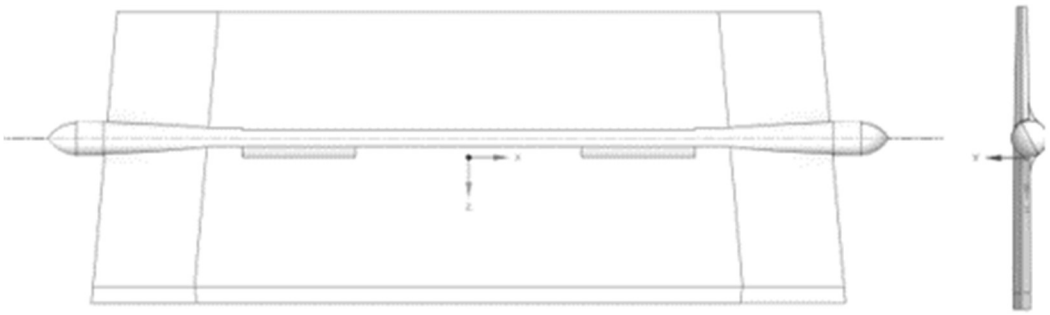

Figure 35 Predesign of Folding Tail Fin

Predesign of an eccentric folding mechanism was drawn where two pieces, rectangular cross shaped torsion spring bars were packed into it.

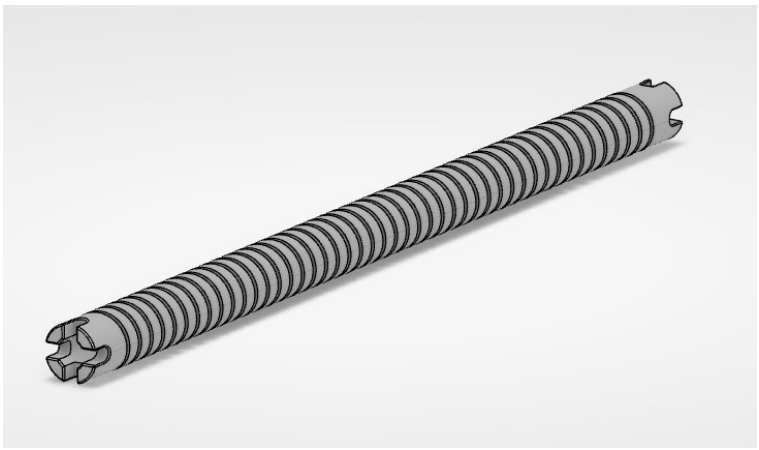

Figure 36 Isometric View of Torsion Spring

4.2. Performed Analyses

4.2.1. Computational Fluid Dynamics Analysis

In this section, a computational fluid Dynamics analysis had been performed on the preliminary airfoil surface which can be seen at figure 33. This airfoil area are the major lifting surfaces at the missile which plays a significant role in missile performance. Because of that reason, there have been studies on designing and optimizing airfoil geometry for ages.

The linearized theory for supersonic flow was first put forward by Ackeret. His assumptions were based on airfoil is thin and the flow is two dimensional. Subsequently this theory was improved by Busemann who also contributed to literature his own name Busemann constant. It is proved that the results of linearized theory are fairly accurate for moderate Mach numbers.[23]

Studies suggest that, straight wing planform is one of the most preferred geometries in airfoil design because of its aerodynamic efficiency, structural weight and cost of manufacturing

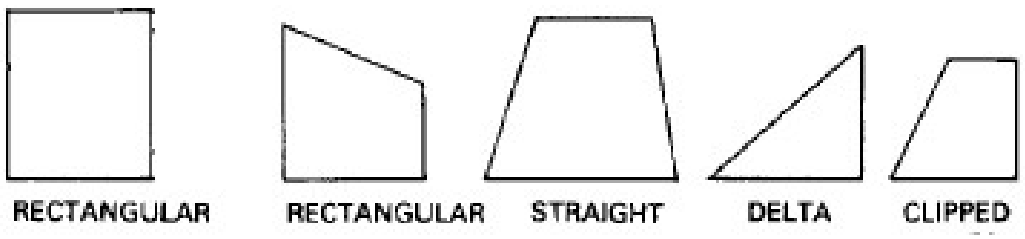

Figure 37 Typical Wing Planforms[2]

Another important airfoil geometry is airfoil cross section geometry. The pressure over an airfoil is a function of angle between fluid direction and surface. In general, sharp nosed symmetrical double wedge airfoil sections result in the most efficient aerodynamic design.

In this thesis, design of an airfoil has been conducted according to well-proven straight edge, modified double wedge geometry. Other than typical planform, an eccentric orthodox folding mechanism has been implemented in the mid surface of the tail fin.

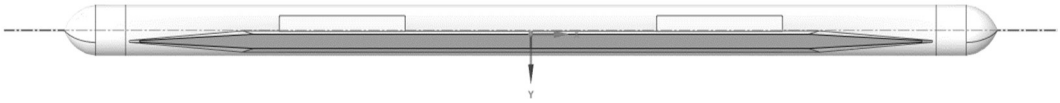

Figure 38 Modified Double Wedge Airfoil Section

After deciding the airfoil geometry, model was created in SpaceClaim environment. Surface preparations were done before analysis in SC. In order to observe fluid separation properly, small surfaces like leading edges, conical surfaces and trailing edges were grouped by named selection for further use.

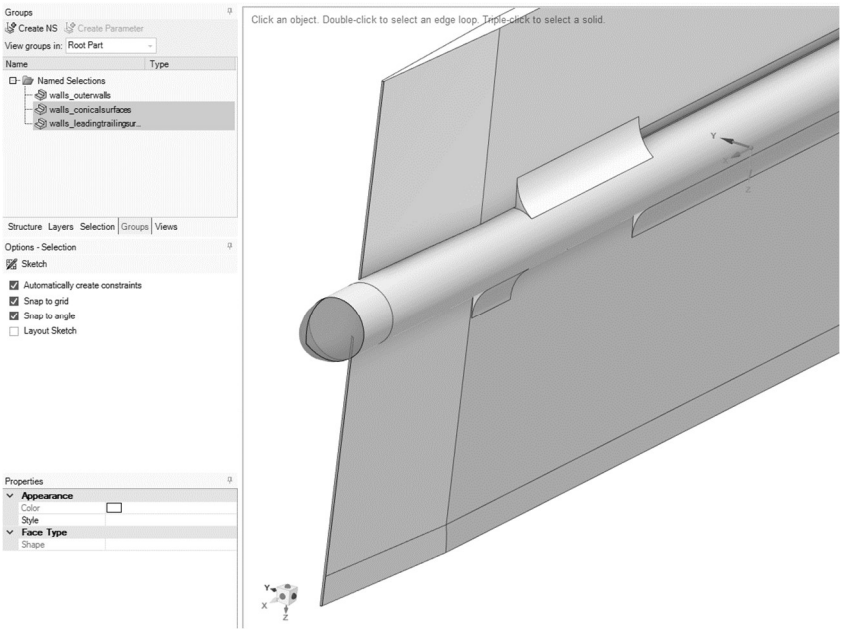

Figure 39 Named Selection of Analysis Model

Unlike structural analysis, external flow CFD analysis differs in a model preparation way. Once the solid body is prepared, one should also prepare the fluid domain by subtracting solid body from the fluid domain. In order to create a suitable fluid domain for an appropriate CFD analysis, one should create at least 5, preferably 10 times greater volume in the corresponding dimension than the original body. In the defense industry, it is best practiced to use the below mentioned dimensions for CFD analysis.

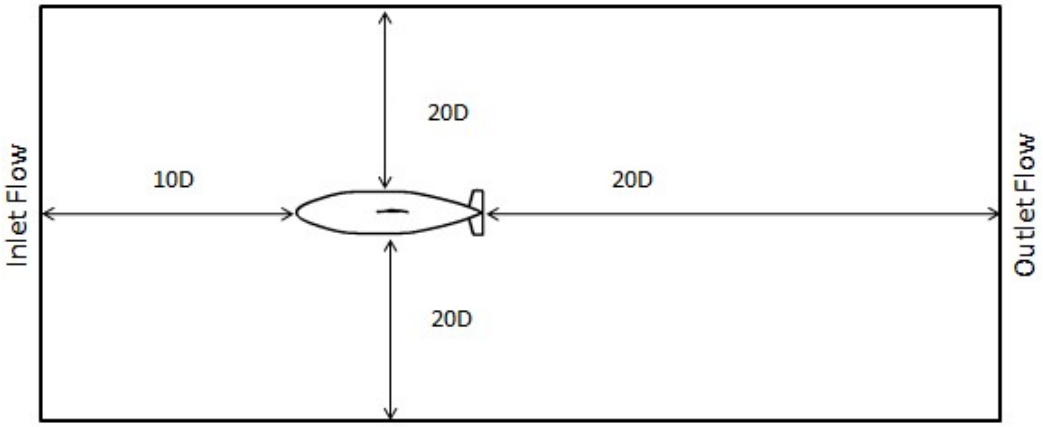

Figure 40 Flow Domain Around the Body

Dimensions of solid body and corresponding fluid domain dimensions are given at table 3 below.

Table 3 Dimensions of the Model

	Solid Body Dimensions	**Fluid Domain Dimensions**
Span	230mm	>20D lateral
Chord	600mm	>10D inlet + 20D outlet
Thickness	30mm	>20D height

All dimensions are chosen far enough where variation of the pressure gradient is insignificant. Far field theory can be used since the distance from the source is much larger than the size of the source itself.

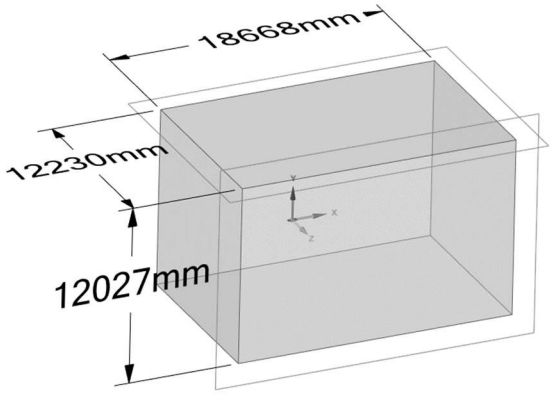

Figure 41 Dimensions of Fluid Domain

Prepared SpaceClaim model was transferred to Ansys Fluent Meshing in order to perform CFD preprocessing.

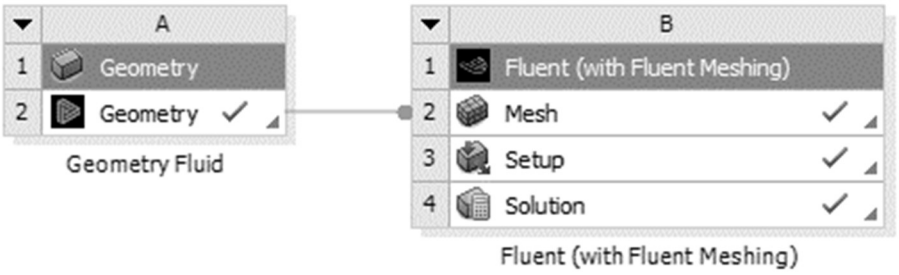

Figure 42 SC Model Transfer to Ansys Fluent Meshing

One should also note that the transferred geometry is not the solid body but the enclosure volume in which it is prepared by subtracting solid body from the fluid domain.

After the model was transferred, local sizing was applied to Named Selections (conical surfaces, leading and trailing edges). Seeing that the local sizing is properly created, surface mesh was created.

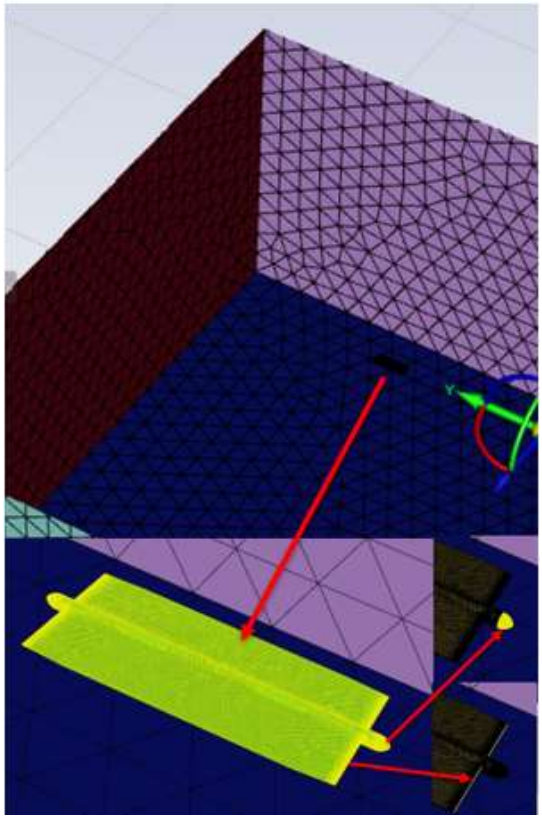

Figure 43 Surface Meshes and Local Sizing

Before creating volume mesh, boundaries and boundary layers should be described to Fluent Mesh. Having subtracted the solid body from the enclosure volume, watertight fluid domain could be created only by fluid regions with no voids.

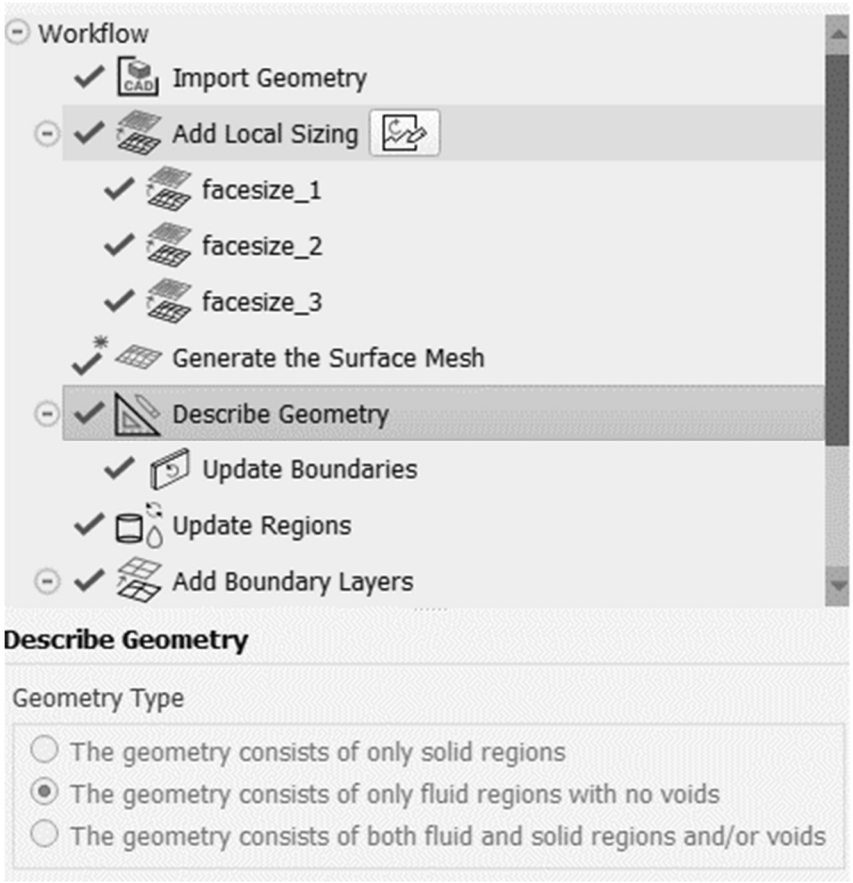

Figure 44 Fluid Region Geometry Type

All boundary types are set as wall except pressure-far-field type for exterior region.

Boundary Name	Boundary Type
mesh_conicalsurfaces	wall
mesh_leadingtrailingsurfaces	wall
wall_innerwalls	wall
zone_farfield	pressure-far-field

Figure 45 Boundary Types

Boundary layer inflation around the folding tail fin should be added between fluid-solid interaction in order to observe external flow separation around the airfoil body. Boundary layer wall thickness is calculated by parameters given below.

Table 4 Wall Distance Estimation Parameters

Temperature	T	300 K
Dynamic Viscosity	μ	1.845e-5 kg/ms
Density	ρ	1.177 kg/m^3
Boundary Layer Length	D	0.6 m
Free stream Velocity	U_∞	1.2 Mach
Dimensionless Wall Distance	y^+	1

Reynolds Number is calculated from:

$$Re = \frac{\rho U_\infty D}{\mu} \tag{4.8}$$

Where Skin friction coefficient is given as Schlichting correlation:

$$C_f = [2log_{10}(Re) - 0.65]^{-2.3} \text{ for Re} < 10^9 \tag{4.9}$$

Wall shear stress is calculated from:

$$\tau_w = \frac{1}{2} C_f \rho {U_\infty}^2 \tag{4.10}$$

Friction velocity is:

$$U_\tau = \sqrt{\frac{\tau_w}{\rho}} \tag{4.11}$$

Finally estimated wall distance is calculated from:

$$y = \frac{y^+ \mu}{\rho U_\tau} \tag{4.12}$$

Table 5 Turbulence Flow Parameters

Reynolds Number	Re	1.6e+8
Skin Friction Coefficient	C_f	1.76e-3
Wall Shear Stress	τ_w	170.48 kg/(ms^2)
Friction Velocity	U_τ	12.03 m/s
Wall Distance	y	1.3e-6 m

Volumetric mesh was created as can be seen below.

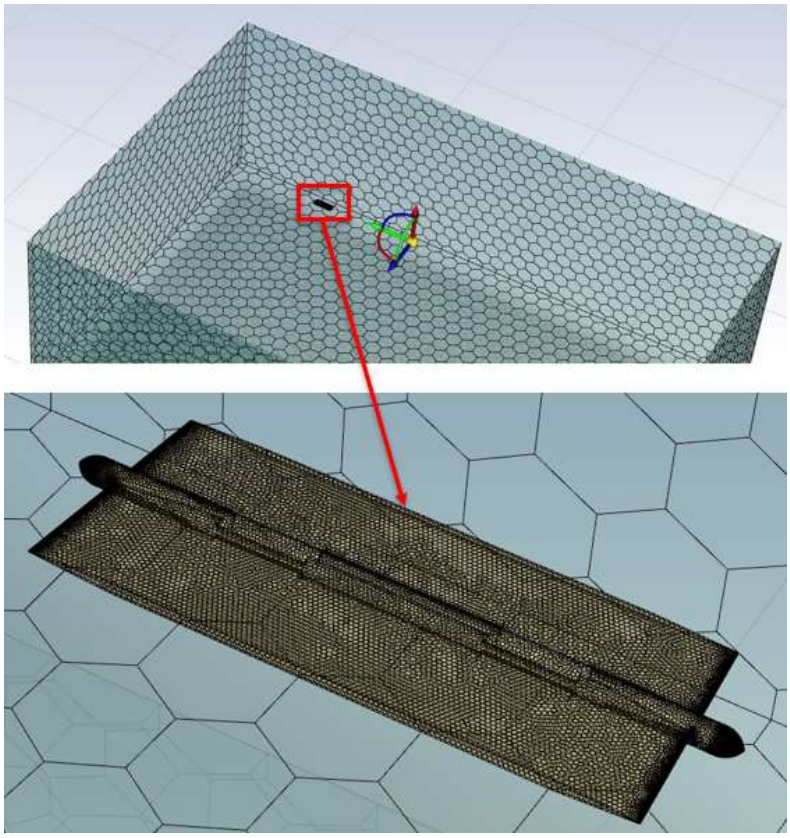

Figure 46 Volumetric Mesh

For a calculated 1.3e-6 m estimated wall distance value and satisfactory 20 boundary layers around the inner walls, meshed model is ready for analysis.

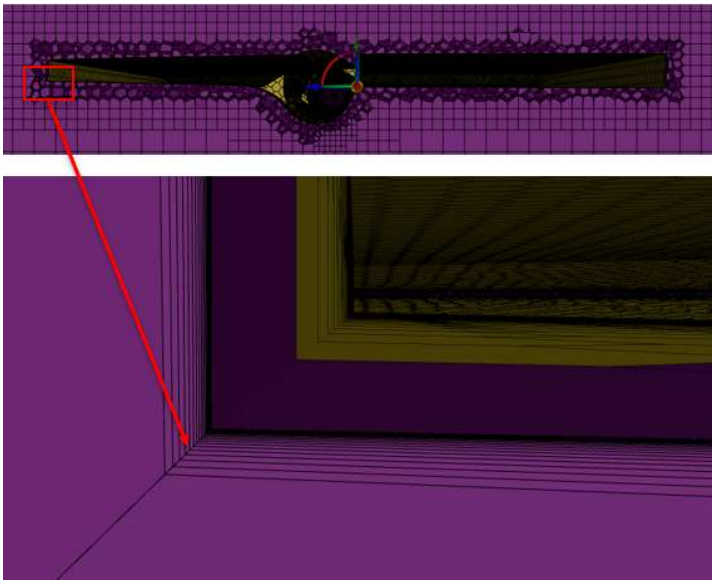

Figure 47 Boundary Layers Around the Walls

Mesh statistics are given at below table.

Table 6 Mesh Statistics

Nodes	3060626
Edges	10093
Faces	6016580
Cells	1534858
Average surface quality, skewness	0.023616

Skewness ratio between 0-0.25 is considered excellent so that we can continue solving process with created model.

First step of solution process is to define rectangular fluid domain as far-field boundary condition to model external flow as free stream condition at infinity where the flow is considered to be undisturbed by the presence of the body.

The pressure far-field boundary condition is often called a characteristic boundary condition, since it uses Riemann invariants to determine the flow variables at the boundaries. This boundary condition is applicable only when the density is calculated using the ideal gas law.

From materials segment, fluid properties are specified ideal-gas for density and Sutherland for viscosity suitably to ensure pressure far-field boundary condition is applicable.

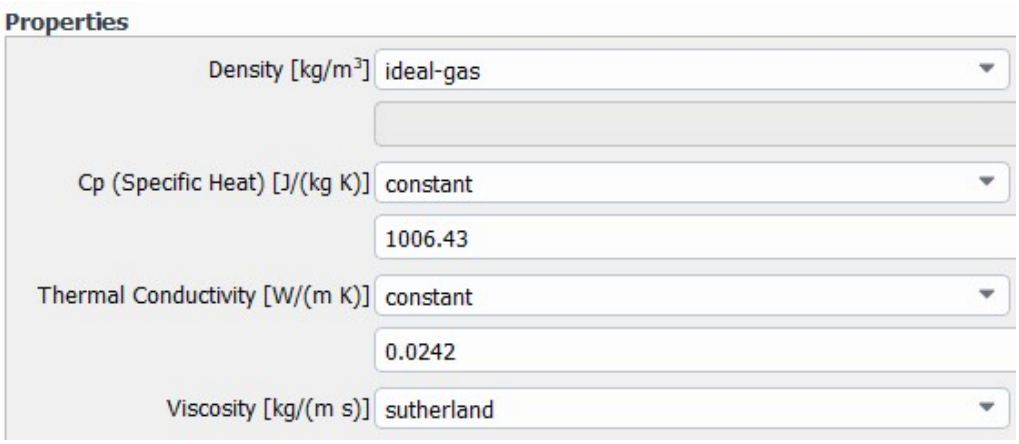

Figure 48 Properties of Fluid

Sutherland viscosity model is a commonly used formula to describe the temperature dependence of the viscosity of a gas. Sutherland's Law is given as:

$$\mu = \mu_0 (\frac{T_0+S}{T+S})(\frac{T}{T_0})^{3/2} \quad (4.13)$$

The Sutherland constant S, is a material specific constant determined from experimental data.

Air viscosity changes as the reference temperature increases as shown below:

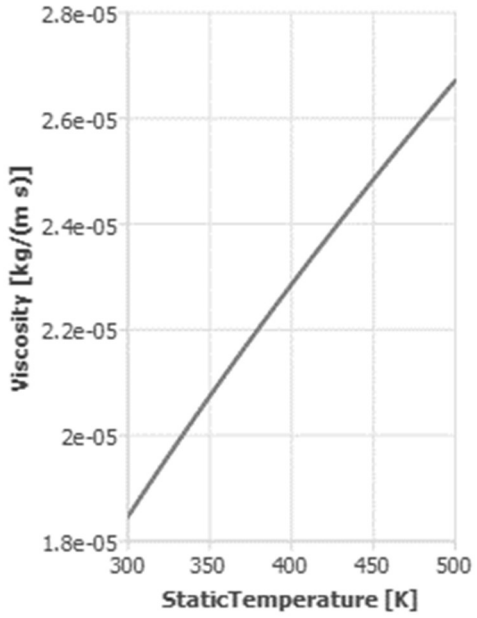

Figure 49 Viscosity Model

Continuing with the necessary setup for pressure far-field condition, static conditions should be specified beforehand.

Remembering that for low supersonic Mach numbers air is calorically perfect. Also, as the speed of the flow approaches the speed of sound, we must consider compressibility effects on the gas. The density of the gas varies from one location to the other.

For calorically perfect gases of isentropic flow, static temperature and static pressure are defined as:

$$\frac{T_0}{T} = 1 + (\frac{\gamma-1}{2})M^2 \quad (4.14)$$

$$\frac{p_0}{p} = [1 + (\frac{\gamma-1}{2})M^2]^{\frac{\gamma}{\gamma-1}} \quad (4.15)$$

Static condition parameters are calculated from below table then found values assigned to far field boundary condition.

Table 7 Static Condition Parameters

Free stream velocity	1.2 Mach
γ	1.4
p_0	101325 Pa
T_0	300 K

Lastly flow direction should be set before analysis. Instead of rotating tail fin according to the Angle of Atack, flow directions are set as a function of AoA.

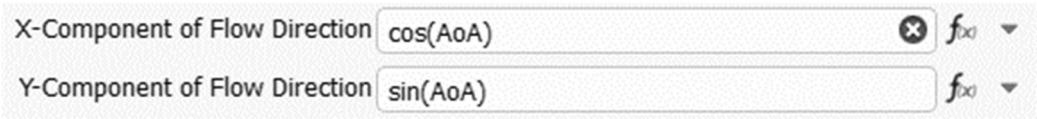

Figure 50 X and Y Components of Flow Direction

Two equation shear stress transport model is used to simulate turbulent flow. This model has two transport equations: one for turbulent kinetic energy and one for the specific rate of dissipation of turbulent kinetic energy. This model provides accuracy and reliability especially for simulating separating flows and flows with adverse pressure gradients.

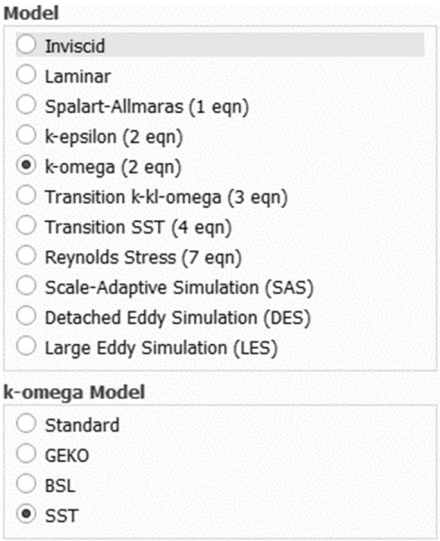

Figure 51 K-Omega SST Model Setup

By using k-omega SST model external flow was analyzed. Pressure distribution on the folding tail fin is determined.

Pressure distribution of upper surface is shown below.

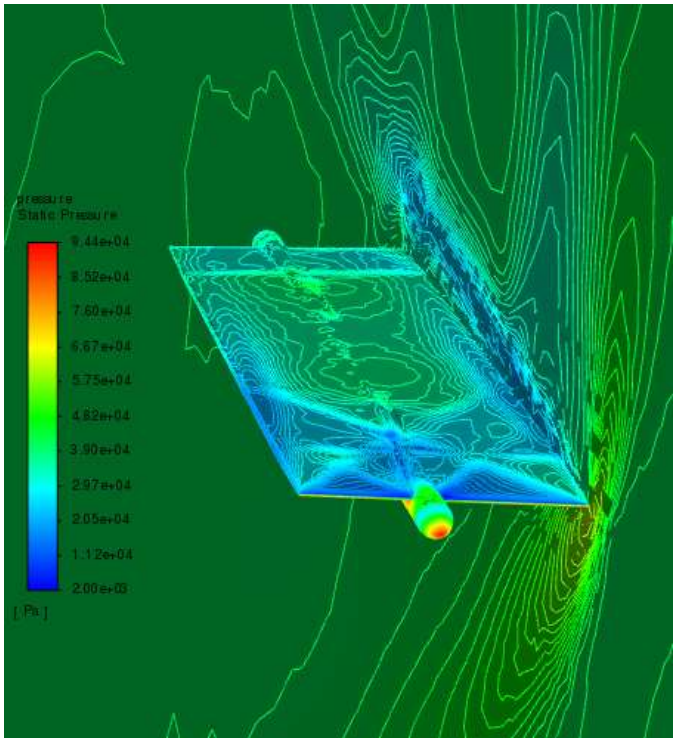

Figure 52 Pressure Distribution of Upper Surface

Pressure distribution of lower surface is depicted below.

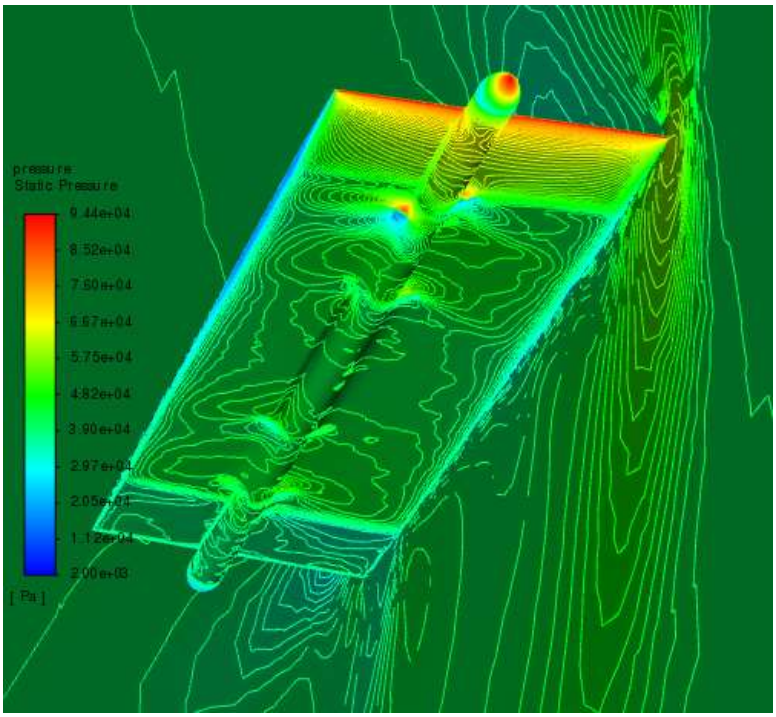

Figure 53 Pressure Distribution of Lower Surface

Additionally, velocity distribution of the bottom tail surface is shared below.

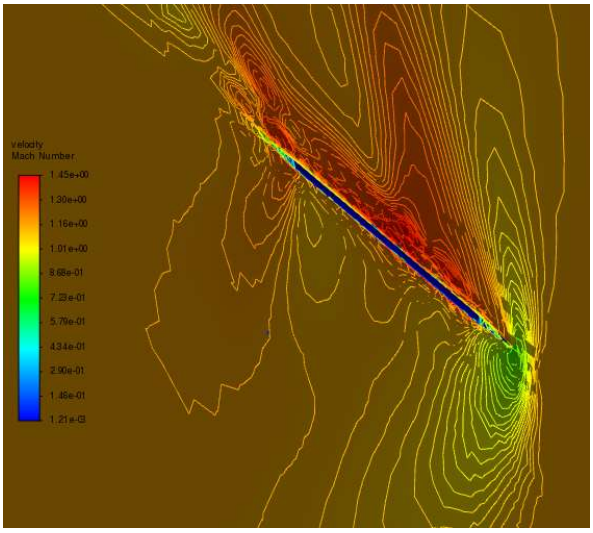

Figure 54 Velocity Distribution of the Bottom Surface

As Bernoulli's Principle states that; for a flow of an ideal incompressible fluid, an increase in fluid speed is associated with a decrease in pressure. This is the basis for lift generation on an airfoil.

When an airfoil is moving through the air at high speeds, the local velocity on the upper surface on the airfoil surpass the free stream velocity where, at the exact spot we can clearly observe pressure drops.

As expected, analyze yields the upper surface of the folding tail fin experiences higher airspeed than lower surface this leads to a decrease in pressure and generation of lift.

Lastly, we should calculate the total lift force and bending moment on the tail fin support. By using Fluent built-in Lift Force and Moment commands, they are calculated as,

```
                  fl
--------------------
                              Lift                     [N]
---------------------------------- --------------------
                                fl              1767.2388

              moment
--------------------
                            Moment                   [N m]
---------------------------------- --------------------
                            moment              202.90361
```

Figure 55 Lift Force and Bending Moment Values

4.2.2. Structural Analysis

After simulating external flow over the folding tail fin, it is essential to analyze how the solid body responds to the fluid forces and pressures. Those can be achieved by performing a fluid to solid interface analysis.

In Ansys workbench Fluent solution is exported to the static structural setup while linking the solid body to the geometry section. Remembering that in CFD section only the fluid body was used as fluid region. We could have used both solid and fluid bodies however it requires shared topology and increases calculation time. For the sake of simplicity, pressure data acquired from Fluent is mapped on the solid body under static structural section.

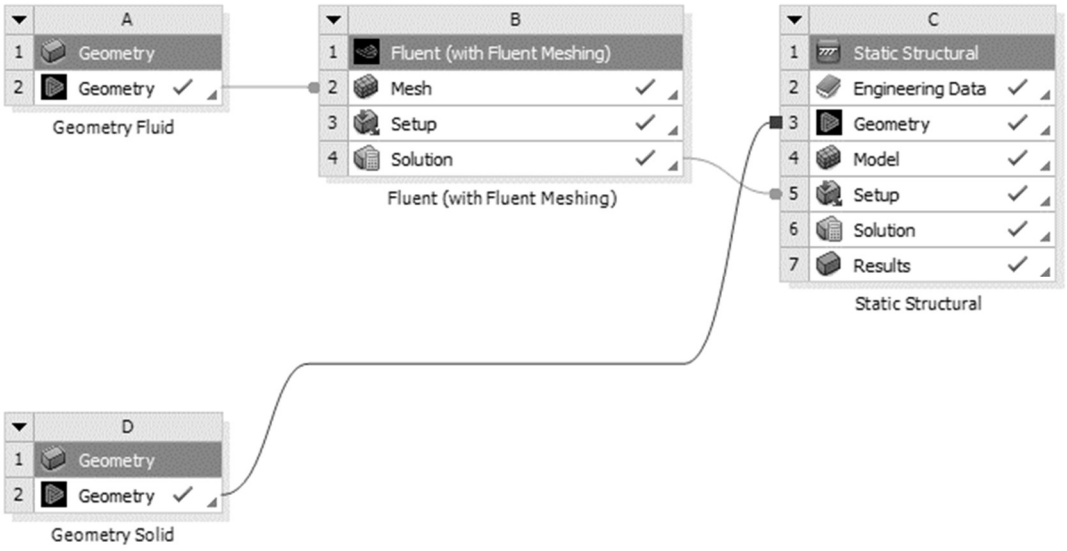

Figure 56 FSI Analysis Model

Static structural preprocess stage is similar to CFD. Geometry is transferred from SC and aluminum is assigned as material property.

Since the solid geometry is fairly small, body sizing is applied on the whole body with an element size of 3mm.

Bottom of the folding tail fin is restrained from all DOF as fixed support.

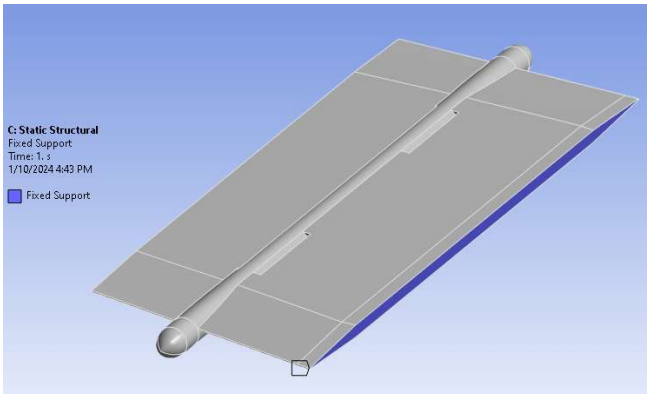

Figure 57 Fixed Support Boundary Condition

Aerodynamic loads exported as statical load and applied on the whole surfaces at the initial time step.

Imported Pressure

	Source Time (s)	Source Time Step	Analysis Time (s)	Scale	Offset (MPa)
1	0.	-1.	1	1	0
*					

Figure 58 Imported Pressure Initial Time Step

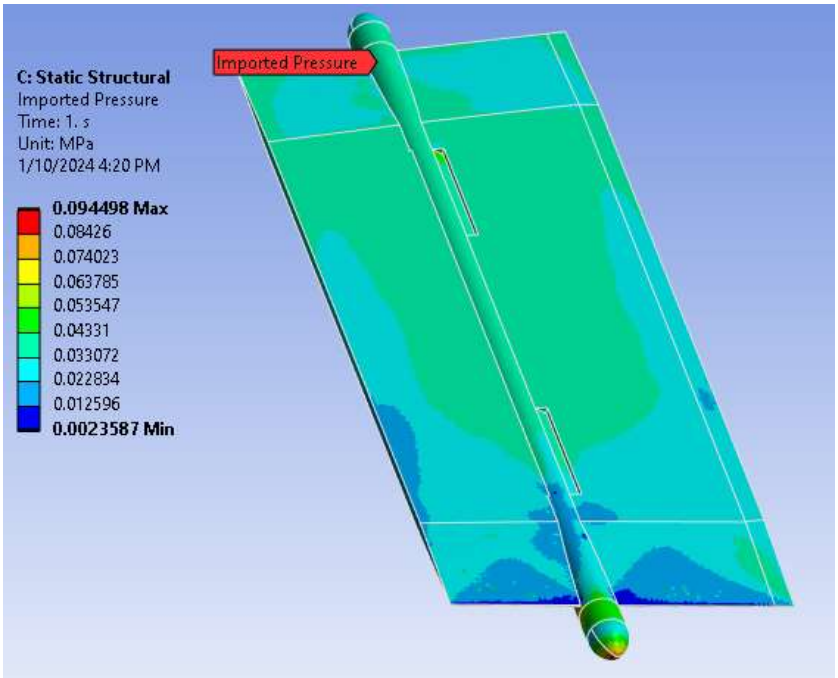

Figure 59 Imported Aerodynamic Pressures

Preprocess stage is summarized below,

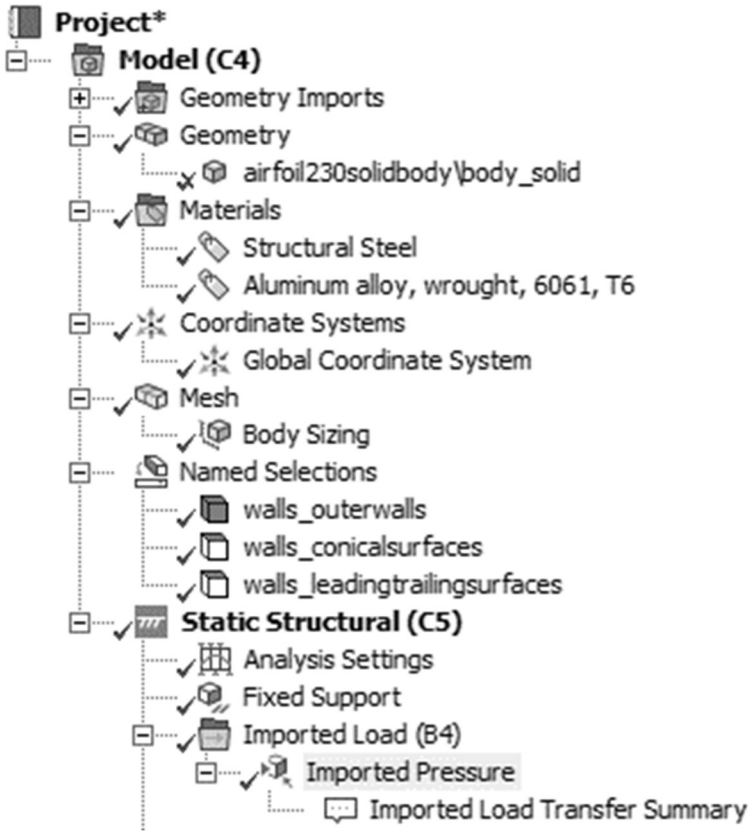

Figure 60 Static Structural Preprocess Setup

Mest metrics are also given as,

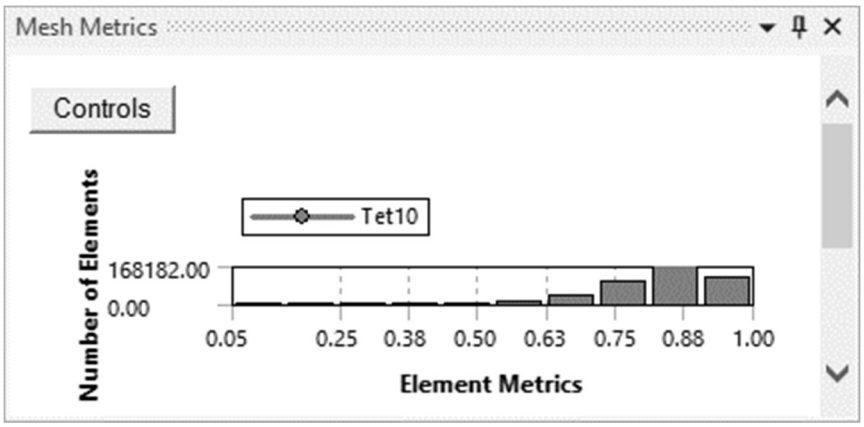

Figure 61 Element Quality

Solid body is discretized with only tetrahedron elements, number of elements are 424015, whose element qualities range between 0.5-1.00. It indicates that there is still room for improvement for better mesh since element quality is recommended to be higher than 0.6. However, number of elements between 0.5-0.6 is very small, it is assumed to be reasonable to continue post process stage with current setup not to increase process time.

In the post process stage; stress, deformation, reaction forces and reaction moments shall be evaluated.

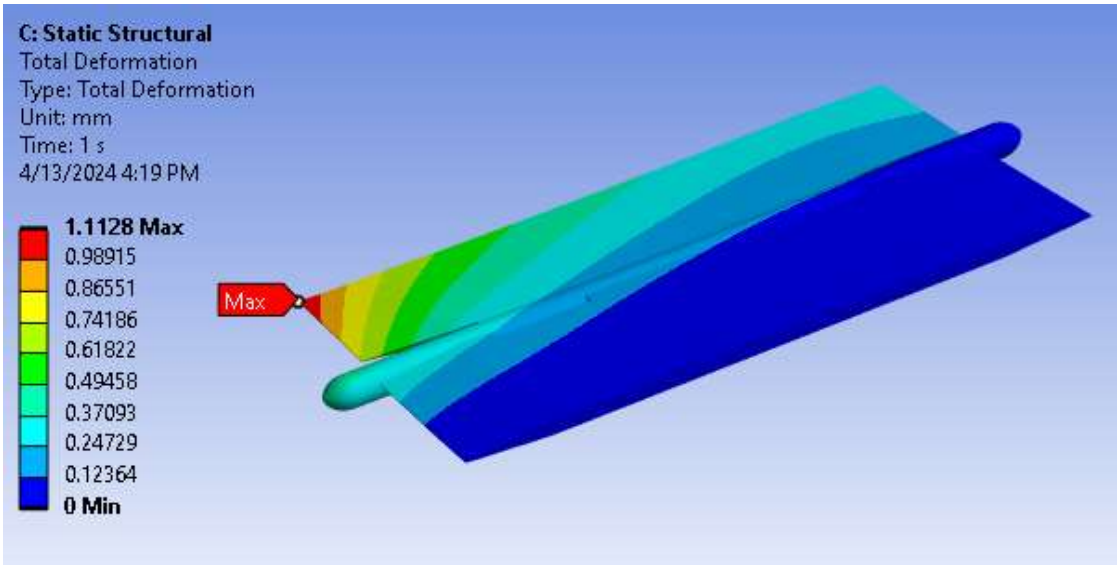

Figure 62 Total Deformation of Folding Tail Fin

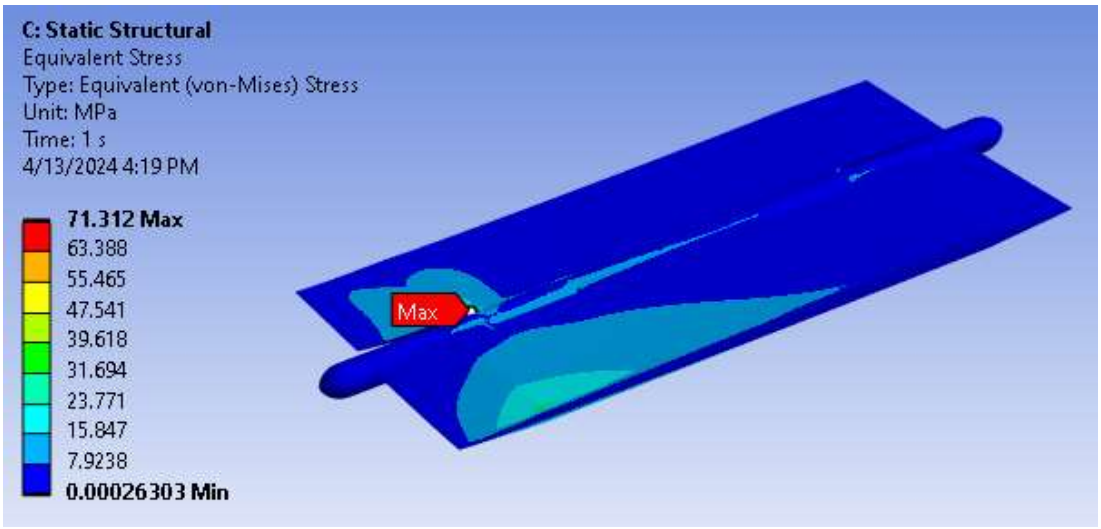

Figure 63 Equivalent Stress Distribution on the Airfoil Body

It is seen that maximum deformation occurs at the tip of the leading edge. On the other hand, lesser deformation occurs at the trailing edge as expected.

Also, maximum von-Mises stresses occur close to the leading edge. For the upper body, it is at the root of folding axis. For the bottom body, it is in the vicinity of the bottom surface. Nevertheless, stress induced by aerodynamic forces are under the yield strength of the aluminum.

Reaction force and reaction moment at the fixed support should also be examined. In physical world, that area corresponds to mating surface of the folding tail fin to the composite booster motor. In the performed test section, validation test in accordance with analysis output will be carried out.

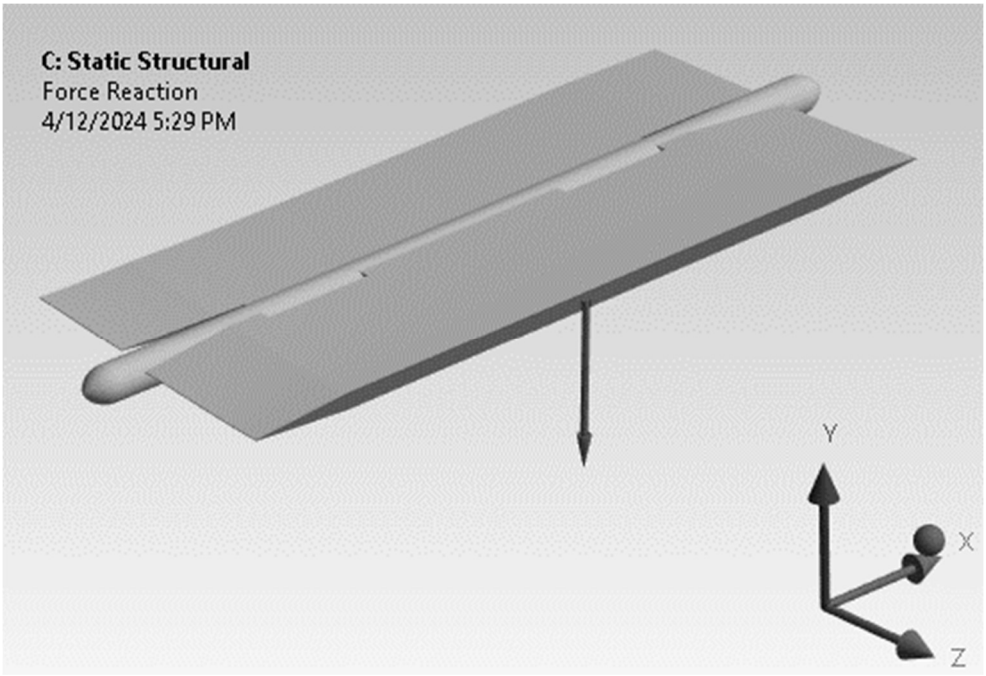

Figure 64 Reaction Force of the Airfoil

Force and moment reaction at support surface is given below.

Table 8 Force and Moment Reaction at Fixed Support

Force Reaction (Y) [N]	-1753.3
Moment Reaction (X) [Nmm]	-2.0092+005

Results obtained from structural analysis are %1 percent different than the lift and moment data calculated by CFD commands. Although this difference is negligible, validation test is conducted according to higher values.

4.2.3. Dynamic Analysis

Completing static analyses, next step is to dynamic analyze airfoil body during release. Deployment time and impact shock could be determined by such an analysis. MSC Adams is found to be suitable for this task.

In the first step 3D model is transferred to MSC Adams platform.

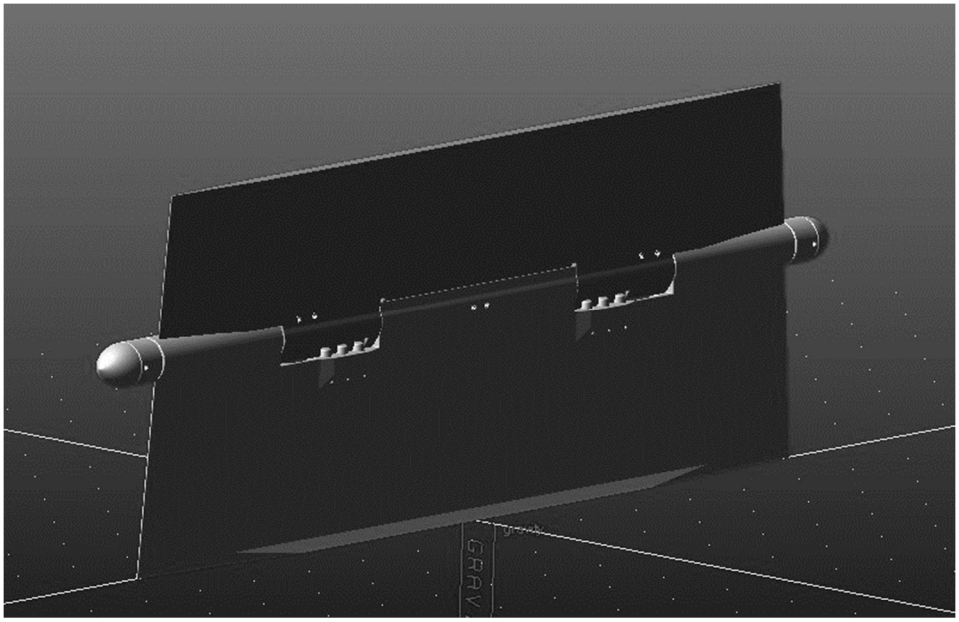

Figure 65 3D Model on MSC Adams

In the second step unnecessary parts which are not mandatory in analysis are deactivated.

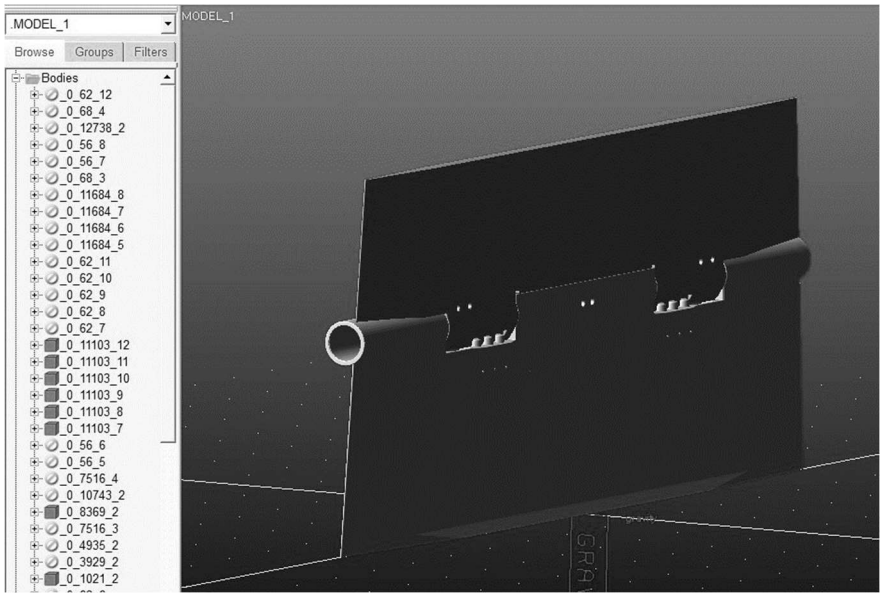

Figure 66 Simplified Dynamic Model

Only lower body, upper body and trunnion locks were left. Moreover, square section torsion bar and compression springs are deactivated too. For illustration purpose springs are depicted below.

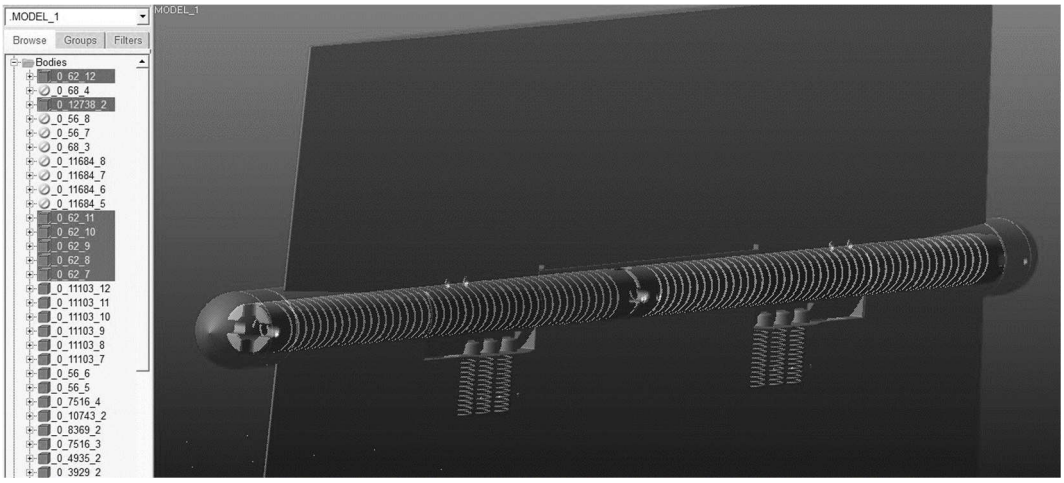

Figure 67 Torsion Springs and Compression Springs

Despite their physical illustrations, related torsion spring and compression spring assignments are made by creating flexible connections.

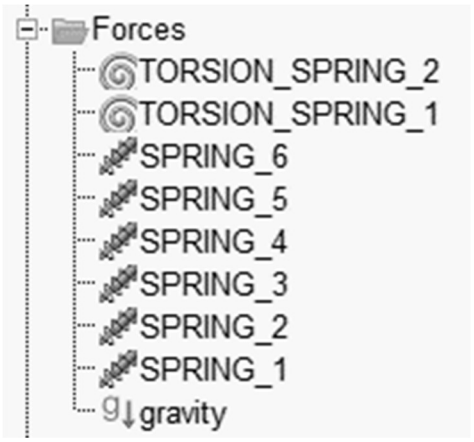

Figure 68 Flexible Connection Assignments

Springs data is shown below;

Table 9 Spring Constants

	Spring Constants
Torsion Springs	2.94 Nm/rad
Compression Springs	3560 N/m

Aluminum is assigned for both lower and upper bodies. For trunnion locks, steel is assigned. Mass and inertia values are automatically calculated afterwards.

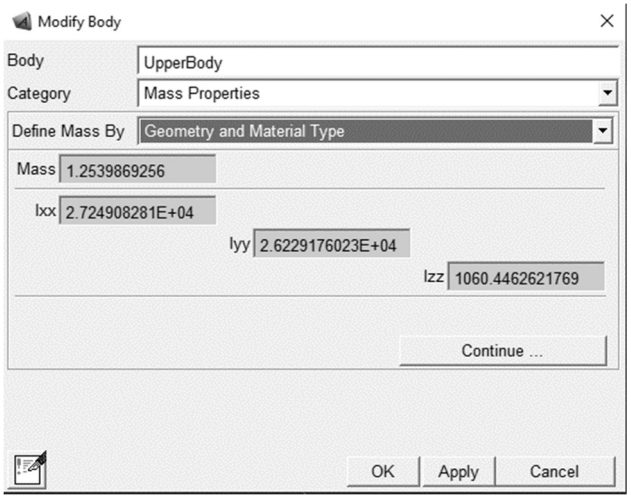

Figure 69 Material Assignment

Degree of freedoms of airfoil bodies are restricted according to the below table.

Table 10 Joint Assignment of the Airfoil Bodies

	Joint Types
Lower Body	Fixed Joint
Upper Body	Revolute Joint
Trunnion Locks	Translational Joint

According to the input parameters, a dynamic analysis is conducted. It is found that 42ms is required for a full stroke of 135° angular displacement from folded to unfolded position.

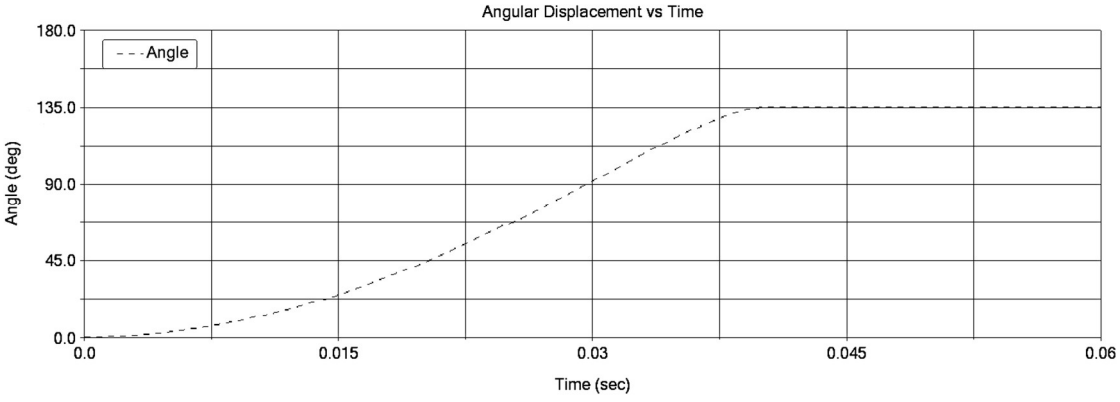

Figure 70 Deployment Time

4.2.4. Fatigue Analysis

To predict the performance and lifespan of torsion bar under cyclic loading where torsion bar is subjected to repeated stress over time, fatigue analysis has to be performed.

The base of fatigue analysis requires the S-N diagram of the material. S-N diagrams represent the relationship between cyclic stress and the number of cycles to failure for a given material.

Torsion spring is manufactured from 17-4 Ph stainless steel, heat treated to H-1050 condition.

Its fatigue properties are given[24],

Stress Ksi	Cycles to Failure		Specimen No.
130	80,000		18
120	261,000		15
110	663,000		16
105	2,053,000		17
105	2,431,000		22
103	531,000		19
103	822,000		20
100	550,000		23
98.5	1,317,000		28
97.5	13,866,000	Runout	27
95	1,713,000		24
95	11,643,000	Runout	21
94	7,800,000		30
93	12,801,000	Failure	26
91	13,267,000	Failure	29
90	16,504,000	Runout	25

Figure 71 Fatigue Properties of 17-4 PH H-1050 Stainless Steel

Those tabulated data manually input to the material properties to create S-N curve.

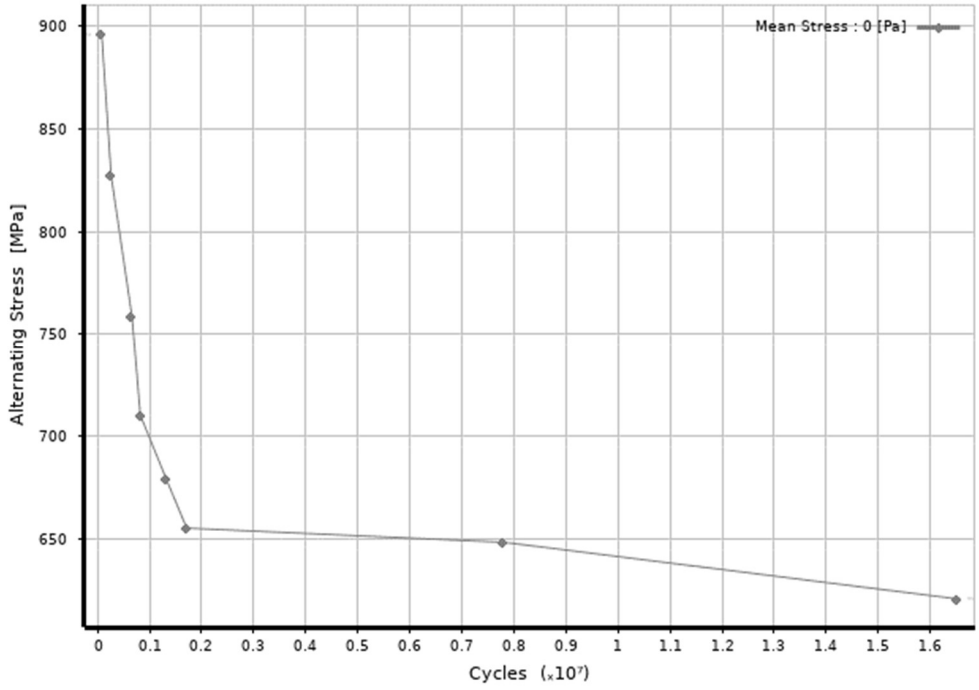

Figure 72 S-N Curve of 17-4 PH H-1050 Stainless Steel

Torsion spring model is transferred to Ansys Structural Environment. Tailored 17-4 PH H-1050 material data assigned to the model.

Having completed the initial setup, CAD model was discretized into smaller pieces. Mesh refinement is applied on the helical surfaces.

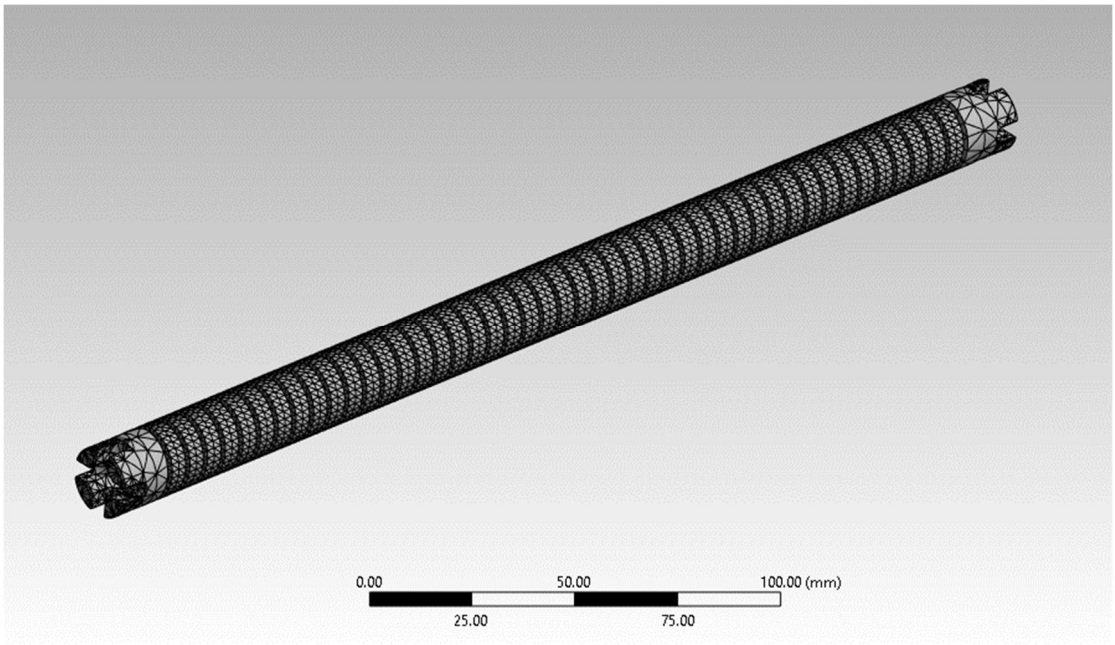

Figure 73 Discretization of the Torsion Spring

Torsion spring is used in folding mechanism in compliance with a bushing. Bushing helps in providing smooth rotation and reduction in friction. Bushing is basically a cylindrical support for torsion spring which provides both sliding and rotation interface.

Another interface of torsion spring is the coiled spring pin interface. Torsion spring is secured from rear end to the airfoil body by the help of coiled spring pin. A coiled spring pin is a mechanical fastener which secures the position of two parts relative to each other.

Two of the torsion spring interfaces are explained above. A fixed supports are applied at rear end mimicking the coiled spring pin and a cylindrical support is applied for outer surfaces, simulating the bushing.

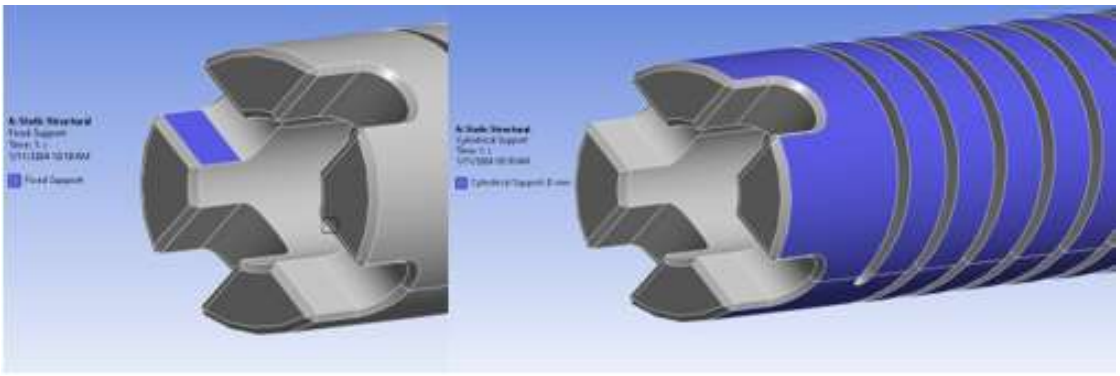

Figure 74 Boundary Conditions of Torsion Spring

Moment produced by torsion springs are applied around the neutral axis as zero-based cycling loading. Stress life analysis type is chosen.

Details of "Fatigue Tool"

Domain	
Domain Type	Time
Materials	
Fatigue Strength Factor (Kf)	1.
Loading	
Type	Zero-Based
Scale Factor	1.
Definition	
Display Time	End Time
Options	
Analysis Type	Stress Life
Mean Stress Theory	Soderberg
Stress Component	Equivalent (von-Mises)
Life Units	
Units Name	cycles
1 cycle is equal to	1. cycles

Figure 75 Fatigue Analysis Settings

As mean stress theory, Soderberg's line is chosen as it is the safest and more conservative approach.

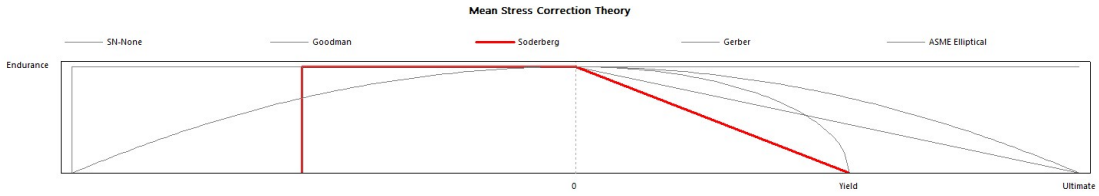

Figure 76 Mean Stress Correction Theory

Once the analysis is run, equivalent stress is calculated as;

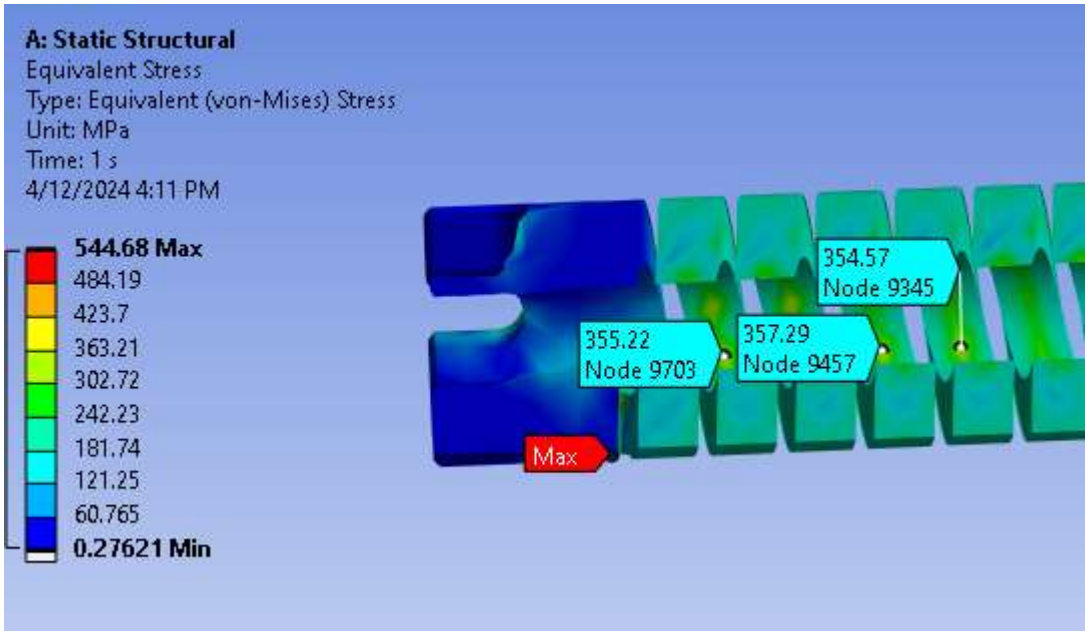

Figure 77 Equivalent Stress Distribution on Torsion Spring

Stress level at the core of the helical coils are observed around 350 MPa which is well below the endurance limit of 17-4PH H-1050 material. Hence it is considered to have infinite life.

Maximum stress is found in the vicinity of beginning of the helix edge; by rounding sharp corner in order to decrease stress concentration at that area significantly reduced stress level below yield stress.

Undeformed and deformed bodies are superimposed in single scene then directional deformation on X axis is plotted below,

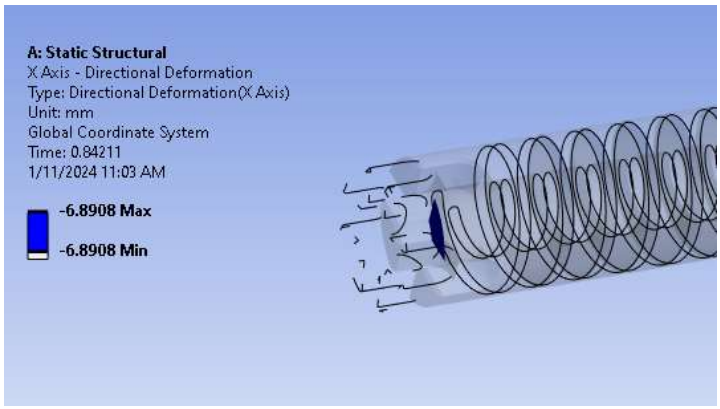

Figure 78 Directional Deformation on Torsion Spring

Torsion spring compresses 6.89mm under the applied torque. Since torsion spring is restrained from rear end but it can make a reciprocating motion from the front that value is important for design perspective to decide the tolerance between mating parts.

Lastly fatigue analysis result is depicted below,

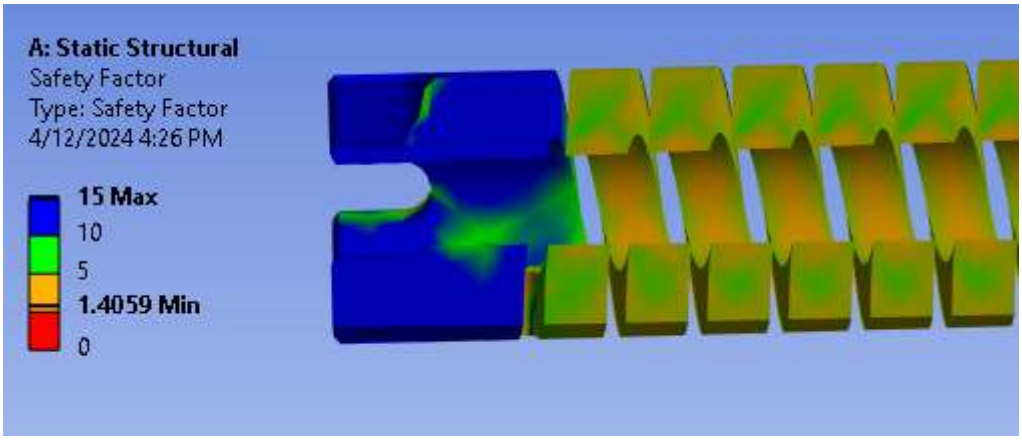

Figure 79 Safety Factor of Torsion Spring

Safety factor is calculated ~1.4 at the core of helical coils which are subjected to the all cycling loading. However, the lowest safety factor is found at the beginning of the coil spring where abrupt change in the part takes place. It should be noted that, at that area; sharp corner should be avoided, fillet radius should be used instead.

4.3. Performed Tests

4.3.1. Aerodynamic Loading Test

Having the aerodynamical pressures on each element over the airfoil body in Ansys, we can transfer those data to an excel file for further calculations.

The necessity of tailoring the aerodynamical pressures has risen from the fact that the airfoil body compose of two different bodies, upper and lower bodies. In order to observe strength of the particular part, Cp of each part should be calculated.

More than 80000 elements and their related pressure and distance values were transferred to excel. Brief representation can be seen below.

Table 11 Exported Aerodynamical Pressure Data of Each Element

Element Number	Face Index	Centroid X (mm)	Centroid Y (mm)	Centroid Z (mm)	Imported Pressure (MPa)
169911	2	290	2.4181	-10.268	0.03
118982	0	290	5.2852	-21.221	0.03
92112	0	290	0.79245	-14.017	0.03
157804	2	290	-8.363	-19.436	0.04
169998	0	290	-5.4451	-21.973	0.04
381080	2	290	-3.3999	-15.93	0.04
92113	3	290	-3.8346	-14.331	0.04
170564	2	290	-0.71953	-8.1217	0.04
92101	2	290	-0.25422	-21.795	0.04
169980	3	290	-1.5275	-11.592	0.04
162863	3	290	4.4009	-14.462	0.03
149538	0	290	-7.3226	-16.664	0.04
149474	0	290	-6.5993	-11.999	0.04
250224	0	290	1.8324	-19.436	0.03

After tailoring the exported data, suitable for upper body and lower body, two different Cp values are found.

Table 12 Cp & Fn Values of Upper and Lower Airfoil Body

	x [mm]	z [mm]	Normal Force [N]
Cp_lower	-187.039	-51.15	794.8
Cp_upper	-168.039	-166.85	972.4

Folding axis, axis system and point of Cp_lower & Cp_upper are shown below.

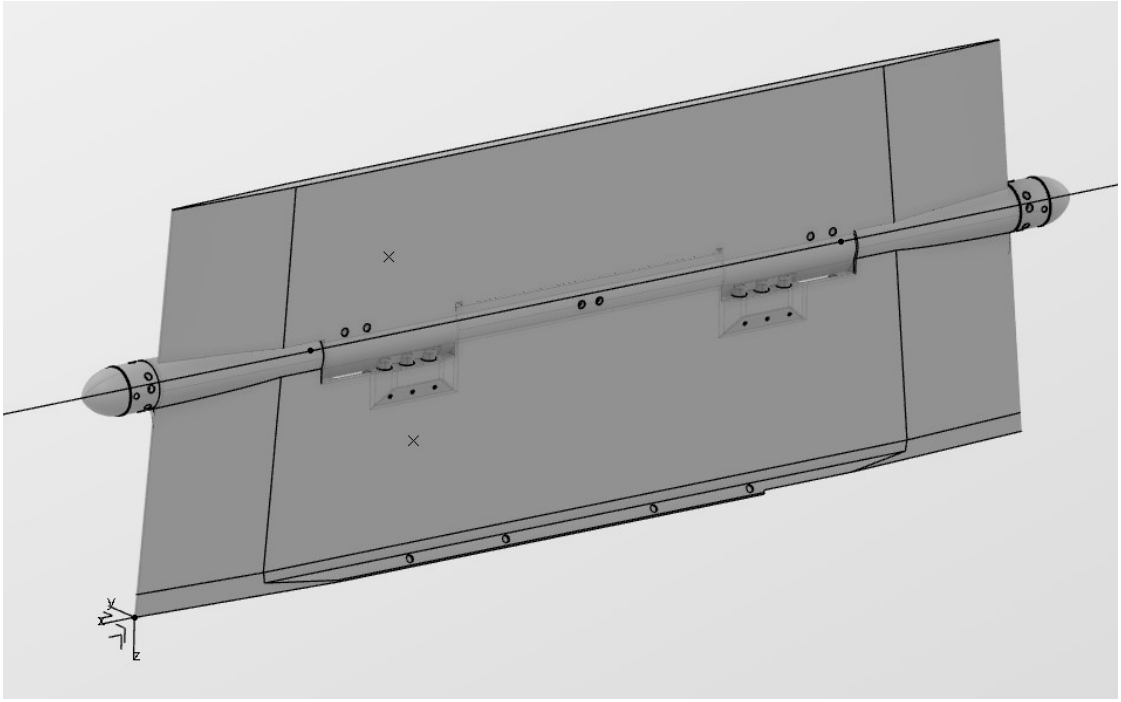

Figure 80 Lower and Upper Cp Points

A test setup was arranged to apply necessary normal force on determined points. Test setup contains fixture, two reciprocating pistons and laser tracker which measures displacements.

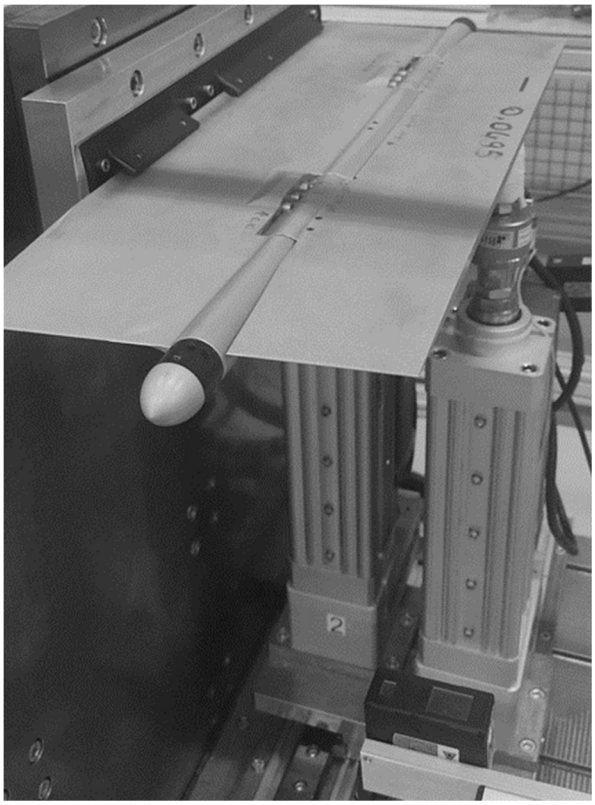

Figure 81 Aerodynamical Loading Test Setup

A test matrix was setup to observe structural integrity of lower and upper body while measuring displacement under applied load. Summary table is depicted below.

Table 13 Summary Table of Aerodynamical Loading Test

Test No	Normal Force [N]	z [mm]	Bending Moment [Nm]	Σ BM [Nm]	Displacement y [mm] @Tip of the leading edge [mm]	Displacement y [mm] @Tip of the trailing edge [mm]	Angle of Twist Φ [°]
1	794.80	51.15	40.65	202.90	1.23	0.16	0.12
	972.40	166.85	162.24				
2	1400.00	51.15	71.61	305.20	1.65	0.23	0.16
	1400.00	166.85	233.59				
3	1850.00	51.15	94.63	403.30	1.93	0.26	0.19
	1850.00	166.85	308.67				

Test was conducted according to the output of aerodynamical loadings data. Displacement at the tip of the leading edge was found as 1.23mm which is within the 1% error margin comparing to structural analysis. Hence it can be said that the findings drawn from analysis align with the outcomes of the test conducted. Furthermore, two more iterations were run up to 1.98 factor of safety. This implies that the data obtained reinforcing the validity and reliability of the developed system.

4.3.2. Structural Integrity Test

In the analysis section, it was calculated that approximately 200Nm bending moment occurs in the vicinity of folding tail bearing surface.

To examine the structural integrity of said surface, a test was conducted. Test setup compose of 3 different units; folding tail fins, dummy weights and inert booster motor.

At the tip of the fin surface, dummy weights are placed generating the desired bending moment at the root of the fin-booster interface.

Figure 82 Structural Integrity Test

Structural integrity test was repeated with different dummy weights. Summary of the test results are given below.

Table 14 Structural Integrity Test Results

Test No	Total Weight [kg]	Bending Moment [Nm]	Load Percentage [%]
1	50	107.91	53
2	100	215.82	106
3	150	323.73	159
4	200	431.64	212

4.3.3. Deployment Time Test

In order to compare analytically calculated deployment time to operational deployment time, a test setup was designed.

It is simply a fixture which holds folding tail fin stationary while quickly releasing the upper folded body, by the help of motor driven actuator, from folded angle to deployed angle. A slotted angle gauge is placed at the rear end to record corresponding fin movement for each time interval.

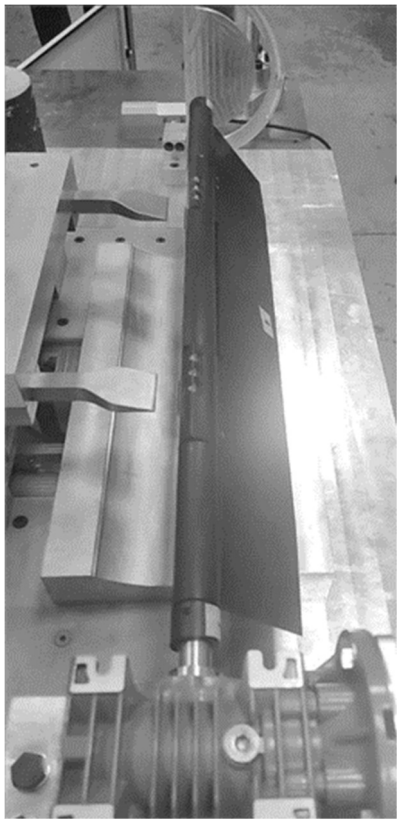

Figure 83 Deployment Time Test Fixture

The test setup was enriched by high-speed camera which records 5000 frames per second. High speed camera recorded the movement of folded tail fin from fully folded angle to deployed angle.

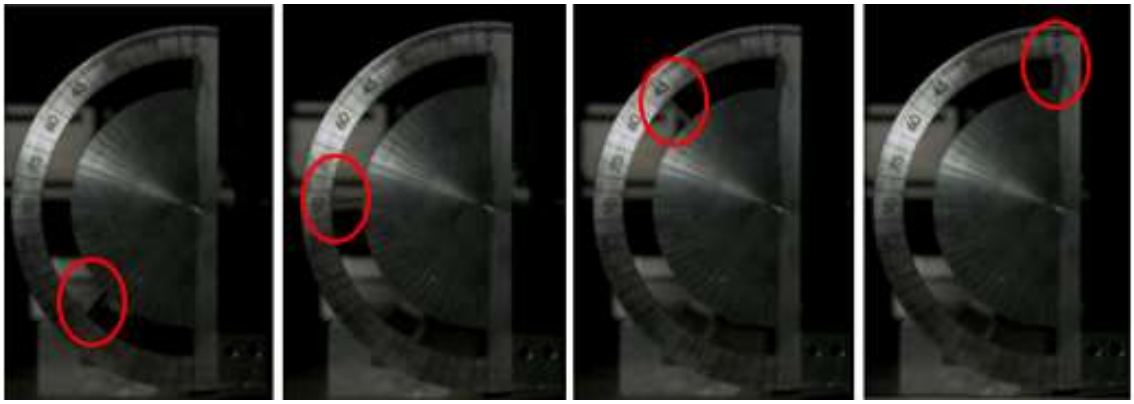

Figure 84 Fin Position for Different Angles

Test results are given below the table.

Table 15 High Speed Camera Deployment Time Test Summary

Frame per second	5000
Total Angle [deg]	135
Total frame	232
Total deployment time [ms]	46.4

Detailed outputs are given at the next table. For each frame, corresponding angle and time were recorded.

Table 16 High Speed Camera Deployment Test Results

Frame	Angle [°]	Time [ms]
68	135	0
102	130	6.8
117	125	9.8
130	120	12.4
142	115	14.8
152	110	16.8

161	105	18.6
169	100	20.2
177	95	21.8
185	90	23.4
193	85	25
200	80	26.4
207	75	27.8
214	70	29.2
220	65	30.4
227	60	31.8
234	55	33.2
240	50	34.4
246	45	35.6
253	40	37
259	35	38.2
265	30	39.4
271	25	40.6
277	20	41.8
283	15	43
289	10	44.2
295	5	45.4
300	0	46.4

A graphical representation of test results is shown below.

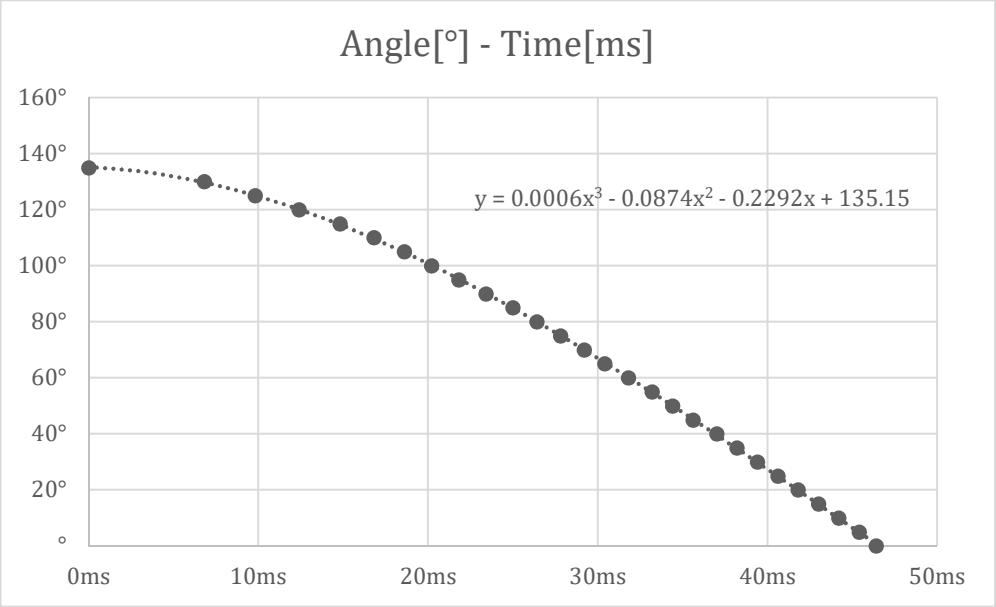

Figure 85 Angle vs Time Graph of Deployment Test

There is a 4ms difference between dynamic analysis deployment time and test result. Considering the fact that there is friction between moving surfaces and there are imperfections during manufacturing process, time difference is at a reasonable stage.

It can be seen from the graph that initial releasing stage takes more time than the final deployment stage which can be further altered by using different spring constants according to the application needs.

From equation 4.4 and relation between torque and moment of inertia, below ODE can be derived;

$$\theta(t) = \left(\frac{\theta_0}{e^{\sqrt{\frac{k}{I}}*t_f} - e^{-\sqrt{\frac{k}{I}}*t_f}} \right) * \left(e^{\sqrt{\frac{k}{I}}*(t_f - t)} - e^{\sqrt{\frac{k}{I}}*(t - t_f)} \right) \tag{4.16}$$

For a known folding angle and deployment time, angular displacement can be calculated with respect to time.

It is apparent that spring constant determines deployment characteristic of folding tail fin significantly.

There are military applications in which deployment time must be in a specific time range such as a missile firing from a launching cell. In order not to interfere with launching cell, upon applications need, slower or rapid deployment can be achieved by altering spring constant.

5. CONCLUSION

In this thesis, comprehensive study for a folding tail fin mechanism is conducted. Object of this study is to develop a folding tail fin mechanism for a tactical missile. In order to achieve this difficult task, studies had been started with literature review. It was seen that there were several different approaches for folding mechanism according to applications need.

Study subjected to this task contains longitudinal folding mechanism. According to our needs, folding mechanism powered by square shaped torsion bar was found to be suitable.

Analytical calculations were made in the preliminary design stage to obtain essential spring data and deployment time. Necessary equations for square shaped torsion bar are presented but overall input parameters such as coil thickness, active coil numbers, coil diameters, spring packaging etc. are not covered in this study.

After analytical calculations, different variety of analysis are performed. Starting with CFD analysis, an external flow over the airfoil body at supersonic speed for low angle of attack is performed.

Calculated aerodynamic pressures were transferred to structural platform for further analyses. Stress on the airfoil body, deformation at the tip of the leading edge, reaction forces and reaction moments in the vicinity of airfoil mating surfaces were determined.

For 17-4 Ph stainless steel heat treated to H1050, fatigue analysis is conducted. Infinite life under cyclic loading is found. However significant stress level is found in the vicinity of beginning of the helix edge. A preventive measure is taken to secure material from fail.

Lastly, analyses are completed by dynamic analysis. Deployment time is calculated. According to performed calculations and analyses, FAI parts are manufactured. Details of the production stage is not covered in this thesis however extensive efforts were spent throughout process stage. Not only airfoil bodies are manufactured but also several fixtures and apparatuses are produced which later on used in the validation tests.

Outputs of fluid to solid interface analyses are verified by aerodynamic loading test and structural integrity test. Together with the deployment time test, dynamic analysis results are validated. A comparison table provided below accurately outlines the deviations between analyses and validation tests.

Table 17 Analyses and Tests Results Comparison Table

	Analyses	Validation Tests	Deviation	Percent Error
Deflection	1.11mm	1.23mm	0.12mm	1%
Deployment Time	42ms	46ms	4ms	9%

In conclusion a state-of-the-art folding tail mechanism is designed. Up to commissioning stage whole exercise is presented. Difference between test data and design data are demonstrated. It can be said that the findings drawn from performed tests, align with the outcomes of the design studies which reinforcing the validity and reliability of the developed system.

For future work, two-way fluid to solid interface analysis can be performed. As missile flies, external flow around the tail fins causes the airfoil body to deform which, in turn, changes the way the air flows, altering the airfoil body even more. Solving the two-way FSI could dramatically increase the aerodynamic performance hence it could significantly increase the confidence level in our design study.

One-way analysis is already performed in this thesis but coupled analysis has yet to be studied.

For the sake of simplicity and reduce computational time, several assumptions were made such as for CFD analysis, only 1 airfoil body was modeled for external flow which will be further improved by modeling whole tactical missile in the fluid domain. That will simulate the turbulent flow over the missile in a preferable way.

Lastly for the material used in folding tail fins, under statical loading, stress induced on the airfoil body is drastically lower than the yield point which indicates an alternative material can be studied. With excellent strength-to-weight ratio, a higher performance can be achieved by selecting composite material. Another advantage of using composite material is to decrease moment of inertia around the rotation axis which decreases total deployment time in a favorable way.

To conclude, starting from preliminary design to validation test; a comprehensive study on developing an ingenious folding mechanism for a tactical missile is carried out. The findings of this thesis study strongly confirm the potential utilization of said mechanism within such a system.

6. REFERENCES

[1] J. W. Boord and B. J. Hoffman, *Air and Missile Defense Systems Engineering*. CRC Press, 2016.

[2] T. V. Karthikeyan and A. K. Kapoor, *Guided Missiles*. Defence Scientific Information Documentation Centre, 1990.

[3] S. S. Chin, *Missile Configuration Design*. McGraw Hill Book Company, 1961.

[4] S. Guptaa and J. Bley, "Folding Configuration for Air Vehicle," 2871005, 2013

[5] J. Shmoldas, C. W. Barlow, and M. B. Hitchings, "Extendable Wing Assembly," EP0811822A1, 1997

[6] J. Lutzenberger, "Folding Wing for a Missile," EP3165870A1, 2017

[7] S. Kongelbeck, "Folding Fin or Wing for Missiles," 2925966, 1960

[8] I. Marburger, D. Howlett, and L. Nagel, "Folding Tail Fins," 3986685, 1976

[9] D. A. Bittle, G. T. Jimmerson, and J. L. Cothran, "Dual-Sliding Fin Lock Assembly," 7552892, 2009

[10] G. T. Jimmerson, "Wing Deployment Device," 4762294, 1998

[11] B. Korn, "Power Operated Folding Wing for Rockets and Missiles," 3563495, 1969

[12] H.-J. Hoeppner, U. Kraemer, and M. Soelter, "Aircraft with Deployable Wing Portions," 4659038, 1987

[13] J. Ball, "Folding Fins," 4323208, 1982

[14] P. M. Crossfield, "Missile Appendage Deployment Mechanism," 4664339, 1987

[15] L. D. Wedertz, "Double Swing Wing Self-Erecting Missile Wing Structure," 4667899, 1987

[16] M. A. Rosenberger, J. J. Ettinger, and B. Shore, "Penguin Missile Folding Wing Configuration," 4717093, 1988

[17] K. D. Thomson, "Deployable Wing Mechanism," 4336914, 1982

[18] A. M. Frank, “Torsion Spring Powered Missile Wing Deployment System,” 4691880, 1987

[19] A. G. Shipunov, L. A. Khripunov, V. M. Kuznetsov, and A. V. Rasskazov, “Folding Wing of Small-Sized Rocket,” 2184339, 2002

[20] V. M. Kuznetsov, A. S. Kapustin, and E. K. Kolonitskij, “Missile Folding Wing,” 2288434C1, 2006

[21] T. T. Smiley, “Missile Fin Unfolding Device,” 4826105, 1989

[22] B. E. Chisolm, “Tail Fin Deployment Device,” 6224013, 2001

[23] J. C. Gunn, “Linearized Supersonic Aerofoil Theory Part I and Part II,” *Royal Society*, vol. 240, no. 820, pp. 327–355, 1947.

[24] M. Raefsky and Boeing Vertol Division, *Fatigue Properties of 17-4 Ph and 15-5 Ph Steel in the H-900 and H-1050 Condition*. Defense Technical Information Center, 1968.

APPENDICES

Appendix A – Approximation of Total Deployment Time

Table A. 1 Angular Velocity and Deployment Time of Subintervals

	Angle[rad]	$\frac{1}{2}k\theta_i^2$	$\frac{1}{2}k\theta_f^2$	$\frac{1}{2}I\omega_i^2$	$\frac{1}{2}I\omega_f^2$	ω_f	Interval Time [s]	Total Time [s]
θ_i	2.356	16.33					0.0000	0.039
	2.339	16.33	16.09	0.00	0.24	10.96	0.0016	
	2.321	16.09	15.85	0.24	0.48	15.46	0.0011	
	2.304	15.85	15.62	0.48	0.72	18.91	0.0009	
	2.286	15.62	15.38	0.72	0.95	21.79	0.0008	
	2.269	15.38	15.15	0.95	1.19	24.32	0.0007	
	2.251	15.15	14.91	1.19	1.42	26.59	0.0007	
	2.234	14.91	14.68	1.42	1.65	28.66	0.0006	
	2.217	14.68	14.46	1.65	1.88	30.58	0.0006	
	2.199	14.46	14.23	1.88	2.11	32.37	0.0005	
	2.182	14.23	14.00	2.11	2.33	34.06	0.0005	
	2.164	14.00	13.78	2.33	2.55	35.65	0.0005	
	2.147	13.78	13.56	2.55	2.77	37.17	0.0005	
	2.129	13.56	13.34	2.77	2.99	38.61	0.0005	
	2.112	13.34	13.12	2.99	3.21	39.99	0.0004	
	2.094	13.12	12.91	3.21	3.43	41.31	0.0004	
	2.077	12.91	12.69	3.43	3.64	42.58	0.0004	
	2.059	12.69	12.48	3.64	3.85	43.81	0.0004	
	2.042	12.48	12.27	3.85	4.07	44.99	0.0004	
	2.025	12.27	12.06	4.07	4.27	46.13	0.0004	

	2.007	12.06	11.85	4.27	4.48	47.23	0.0004	
	1.990	11.85	11.65	4.48	4.69	48.30	0.0004	
	1.972	11.65	11.44	4.69	4.89	49.34	0.0004	
	1.955	11.44	11.24	4.89	5.09	50.35	0.0003	
	1.937	11.24	11.04	5.09	5.29	51.33	0.0003	
	1.920	11.04	10.84	5.29	5.49	52.28	0.0003	
	1.902	10.84	10.65	5.49	5.69	53.20	0.0003	
	1.885	10.65	10.45	5.69	5.88	54.11	0.0003	
	1.868	10.45	10.26	5.88	6.07	54.99	0.0003	
	1.850	10.26	10.07	6.07	6.26	55.84	0.0003	
	1.833	10.07	9.88	6.26	6.45	56.68	0.0003	
	1.815	9.88	9.69	6.45	6.64	57.50	0.0003	
	1.798	9.69	9.51	6.64	6.83	58.29	0.0003	
	1.780	9.51	9.32	6.83	7.01	59.07	0.0003	
	1.763	9.32	9.14	7.01	7.19	59.84	0.0003	
	1.745	9.14	8.96	7.19	7.37	60.58	0.0003	
	1.728	8.96	8.78	7.37	7.55	61.31	0.0003	
	1.710	8.78	8.61	7.55	7.73	62.02	0.0003	
	1.693	8.61	8.43	7.73	7.90	62.72	0.0003	
	1.676	8.43	8.26	7.90	8.07	63.40	0.0003	
	1.658	8.26	8.09	8.07	8.25	64.07	0.0003	
	1.641	8.09	7.92	8.25	8.41	64.73	0.0003	
	1.623	7.92	7.75	8.41	8.58	65.37	0.0003	
	1.606	7.75	7.59	8.58	8.75	66.00	0.0003	
	1.588	7.59	7.42	8.75	8.91	66.61	0.0003	
	1.571	7.42	7.26	8.91	9.07	67.21	0.0003	
	1.553	7.26	7.10	9.07	9.23	67.81	0.0003	

	1.536	7.10	6.94	9.23	9.39	68.39	0.0003	
	1.518	6.94	6.78	9.39	9.55	68.95	0.0003	
	1.501	6.78	6.63	9.55	9.71	69.51	0.0003	
	1.484	6.63	6.48	9.71	9.86	70.06	0.0002	
	1.466	6.48	6.32	9.86	10.01	70.60	0.0002	
	1.449	6.32	6.17	10.01	10.16	71.12	0.0002	
	1.431	6.17	6.03	10.16	10.31	71.64	0.0002	
	1.414	6.03	5.88	10.31	10.45	72.14	0.0002	
	1.396	5.88	5.74	10.45	10.60	72.64	0.0002	
	1.379	5.74	5.59	10.60	10.74	73.13	0.0002	
	1.361	5.59	5.45	10.74	10.88	73.60	0.0002	
	1.344	5.45	5.31	10.88	11.02	74.07	0.0002	
	1.326	5.31	5.18	11.02	11.16	74.53	0.0002	
	1.309	5.18	5.04	11.16	11.29	74.98	0.0002	
	1.292	5.04	4.91	11.29	11.43	75.42	0.0002	
	1.274	4.91	4.78	11.43	11.56	75.86	0.0002	
	1.257	4.78	4.65	11.56	11.69	76.28	0.0002	
	1.239	4.65	4.52	11.69	11.82	76.70	0.0002	
	1.222	4.52	4.39	11.82	11.94	77.11	0.0002	
	1.204	4.39	4.27	11.94	12.07	77.51	0.0002	
	1.187	4.27	4.14	12.07	12.19	77.90	0.0002	
	1.169	4.14	4.02	12.19	12.31	78.29	0.0002	
	1.152	4.02	3.90	12.31	12.43	78.67	0.0002	
	1.134	3.90	3.79	12.43	12.55	79.04	0.0002	
	1.117	3.79	3.67	12.55	12.66	79.40	0.0002	
	1.100	3.67	3.56	12.66	12.78	79.76	0.0002	
	1.082	3.56	3.45	12.78	12.89	80.11	0.0002	

	1.065	3.45	3.33	12.89	13.00	80.45	0.0002	
	1.047	3.33	3.23	13.00	13.11	80.78	0.0002	
	1.030	3.23	3.12	13.11	13.21	81.11	0.0002	
	1.012	3.12	3.01	13.21	13.32	81.43	0.0002	
	0.995	3.01	2.91	13.32	13.42	81.75	0.0002	
	0.977	2.91	2.81	13.42	13.52	82.05	0.0002	
	0.960	2.81	2.71	13.52	13.62	82.35	0.0002	
	0.942	2.71	2.61	13.62	13.72	82.65	0.0002	
	0.925	2.61	2.52	13.72	13.82	82.94	0.0002	
	0.908	2.52	2.42	13.82	13.91	83.22	0.0002	
	0.890	2.42	2.33	13.91	14.00	83.50	0.0002	
	0.873	2.33	2.24	14.00	14.09	83.76	0.0002	
	0.855	2.24	2.15	14.09	14.18	84.03	0.0002	
	0.838	2.15	2.06	14.18	14.27	84.29	0.0002	
	0.820	2.06	1.98	14.27	14.35	84.54	0.0002	
	0.803	1.98	1.90	14.35	14.44	84.78	0.0002	
	0.785	1.90	1.81	14.44	14.52	85.02	0.0002	
	0.768	1.81	1.74	14.52	14.60	85.25	0.0002	
	0.750	1.74	1.66	14.60	14.68	85.48	0.0002	
	0.733	1.66	1.58	14.68	14.75	85.70	0.0002	
	0.716	1.58	1.51	14.75	14.83	85.92	0.0002	
	0.698	1.51	1.43	14.83	14.90	86.13	0.0002	
	0.681	1.43	1.36	14.90	14.97	86.33	0.0002	
	0.663	1.36	1.29	14.97	15.04	86.53	0.0002	
	0.646	1.29	1.23	15.04	15.11	86.73	0.0002	
	0.628	1.23	1.16	15.11	15.17	86.91	0.0002	
	0.611	1.16	1.10	15.17	15.24	87.09	0.0002	

	0.593	1.10	1.04	15.24	15.30	87.27	0.0002	
	0.576	1.04	0.98	15.30	15.36	87.44	0.0002	
	0.559	0.98	0.92	15.36	15.42	87.61	0.0002	
	0.541	0.92	0.86	15.42	15.47	87.77	0.0002	
	0.524	0.86	0.81	15.47	15.53	87.92	0.0002	
	0.506	0.81	0.75	15.53	15.58	88.07	0.0002	
	0.489	0.75	0.70	15.58	15.63	88.22	0.0002	
	0.471	0.70	0.65	15.63	15.68	88.36	0.0002	
	0.454	0.65	0.61	15.68	15.73	88.49	0.0002	
	0.436	0.61	0.56	15.73	15.77	88.62	0.0002	
	0.419	0.56	0.52	15.77	15.82	88.74	0.0002	
	0.401	0.52	0.47	15.82	15.86	88.86	0.0002	
	0.384	0.47	0.43	15.86	15.90	88.97	0.0002	
	0.367	0.43	0.40	15.90	15.94	89.08	0.0002	
	0.349	0.40	0.36	15.94	15.98	89.18	0.0002	
	0.332	0.36	0.32	15.98	16.01	89.28	0.0002	
	0.314	0.32	0.29	16.01	16.04	89.37	0.0002	
	0.297	0.29	0.26	16.04	16.07	89.46	0.0002	
	0.279	0.26	0.23	16.07	16.10	89.54	0.0002	
	0.262	0.23	0.20	16.10	16.13	89.62	0.0002	
	0.244	0.20	0.18	16.13	16.16	89.69	0.0002	
	0.227	0.18	0.15	16.16	16.18	89.76	0.0002	
	0.209	0.15	0.13	16.18	16.20	89.82	0.0002	
	0.192	0.13	0.11	16.20	16.23	89.88	0.0002	
	0.175	0.11	0.09	16.23	16.24	89.93	0.0002	
	0.157	0.09	0.07	16.24	16.26	89.98	0.0002	
	0.140	0.07	0.06	16.26	16.28	90.02	0.0002	

	0.122	0.06	0.04	16.28	16.29	90.06	0.0002	
	0.105	0.04	0.03	16.29	16.30	90.09	0.0002	
	0.087	0.03	0.02	16.30	16.31	90.12	0.0002	
	0.070	0.02	0.01	16.31	16.32	90.14	0.0002	
	0.052	0.01	0.01	16.32	16.33	90.16	0.0002	
	0.035	0.01	0.00	16.33	16.33	90.17	0.0002	
	0.017	0.00	0.00	16.33	16.33	90.18	0.0002	
θ_f	0.000	0.00	0.00	16.33	16.33	90.18	0.0002	